Geochemical Perspectives Letters

Zircon halogen geochemistry: Insights into Hadean-Archean fluids

H. Tang[1*], D. Trail[1,2], E.A. Bell[1], T.M. Harrison[1]

OPEN ACCESS

doi: 10.7185/geochemlet.1905

Abstract

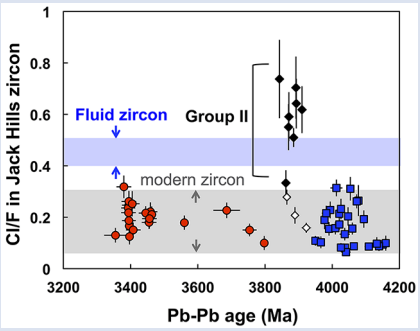

Understanding the distribution of halogens in rocks can potentially trace ancient lithosphere, hydrosphere, and atmosphere interactions. Although no sedimentary rocks older than 3.8 Ga are known, insights into sediment-atmosphere exchange on early Earth could be obtained from knowledge of halogen contents in ancient zircons. Here we present the first study of halogen abundances in Jack Hills zircons together with younger zircons of known provenance to provide geologic context. The relatively low (*ca.* 0.1-0.6 µg/g) chlorine concentrations in most Hadean and Archean Jack Hills zircons are similar to the average concentration in younger igneous zircons. In contrast, significant Cl enrichments are found in a subset of *ca.* 3.9–3.8 Ga zircons ($[Cl]_{average}$= 1.43 ± 0.27 µg/g) that appear to record halogen transport under hydrothermal conditions. Such Cl-bearing fluids in early Earth history may reflect extraction of halogens from the interior to near surface environments.

Received 21 September 2018 | Accepted 20 January 2019 | Published 19 February 2019

Introduction

Earliest Earth remains one of the great frontiers for fundamental discovery as little is known about key events such as the mechanisms and timing of life's origin. Given that >3.8 Ga rocks are exceedingly rare and no rock older than 4.03 Ga is known (*cf.* O'Neil *et al.*, 2008), constraining conditions on early Earth has largely relied on the only materials identified from the Hadean eon: ~4.4 to 3.8 Ga detrital zircons (Mojzsis *et al.*, 2001; Peck *et al.*, 2001; Harrison *et al.*, 2008; Holden *et al.*, 2009; Bell *et al.*, 2011). Oxygen isotopes, rare earth element (REE) patterns, crystallisation temperatures, and inclusions in detrital zircons from the Jack Hills, Western Australia, are suggestive of the presence of recycled crustal material that had interacted with liquid water at low temperature (*e.g.*, Watson and Harrison, 2005; Trail *et al.*, 2011; Bell and Harrison 2013; Harrison *et al.*, 2017) and show how experimental calibrations can permit zircon to act as an environmental monitor of lithosphere and surface processes. On the other hand, the lack of a known sedimentary record older than 3.83 Ga (Manning *et al.*, 2006) limits our understanding of the volatile evolution on earliest Earth. To address this issue, one approach is to trace those volatile components that partition at measureable levels into zircon. Previous investigations of oxygen isotopes and trace elements in Jack Hills zircons (*e.g.*, Mojzsis *et al.*, 2001; Cavosie *et al.*, 2005; Trail *et al.*, 2007; Bell *et al.*, 2011) indicate two distinctive protolith sources: Group I and Group II (Bell and Harrison, 2013). Group I is similar in most respects to >3.9 Ga and <3.8 Ga Jack Hills zircons, with magmatic Th/U and average Ti-in-zircon temperatures *ca.* 680 °C. Group II is a distinctive subset of the zircons with ages 3.9–3.8 Ga that show distinctive chemistry relative to Group I (lower Th/U, P, and Ce; higher U and Hf). Their Ti-in-zircon temperatures are mostly subsolidus, and these zircons are either dark and homogeneous in cathodoluminescence or display patchy zoning. The Group II characteristics imply recrystallisation during thermal events (Hoskin and Black, 2000). Such episodes may have provided a mechanism for volatile transport in early fluids. Given the significance of halogens in lithosphere-hydrosphere-atmosphere interactions, we focus here on their abundances in Jack Hills zircons and examine fractionations between nominally mobile (Cl) and immobile (F) halogens in a variety of reservoirs (*e.g.*, magmatic and metamorphic systems).

Samples and Methods

Our Jack Hills zircon suite ranges in U-Pb age from 4.2 to 3.4 Ga (Table S-2). Oxygen isotope ratios and REE patterns in some of these zircons have been investigated previously and shown to lack secondary alteration (Table S-2, S-3, and S-4, Fig. S-7 and S-8; Bell *et al.*, 2011, 2014, 2016; Bell and Harrison, 2013). Given the possible felsic parent sources of Jack Hills zircon (Bell *et al.*, 2018), zircons from igneous (I-type) and sedimentary (S-type) granitoids from the Phanerozoic Lachlan Fold Belt (LFB), Australia, and Mesozoic batholiths of southern California, USA, were also investigated as

1. Department of Earth, Planetary and Space Sciences, University of California, Los Angeles, Los Angeles CA, 90095 USA
2. Department of Earth and Environmental Sciences, University of Rochester, Rochester, NY, 14618 USA
* Corresponding author (email: haolantang@ucla.edu)

analogues for establishing geologic provenance. Detection limits ([F] = 0.78 ± 0.07 μg/g and [Cl] = 0.12 ± 0.02 μg/g with 2 se.; Fig. S-4) were determined by analysing synthetic zircons grown in halogen-free conditions by the 1 atm flux method (*e.g.,* Trail *et al.,* 2016). We also synthesised zircon grains in a halogen-rich fluid to explore Cl (and F) partitioning in zircon and to produce an analogue of recrystallised zircon (see Supplementary Information for experimental details).

The *in situ* analyses of Cl and F in zircon were performed using the CAMECA *ims*1290 ion microprobe. Analytical details are described in the Supplementary Information. Mud Tank zircons implanted with known F or Cl isotopic dosages were analysed as concentration standards. Cracks/inclusions in samples were identified *via* secondary and backscattered electron SEM imaging. Analysis zones were limited to regions without cracks or inclusions.

Results

Young zircons (1.1–0.1 Ga) display uniform F concentrations (Fig. 1) within uncertainty (1.80 ± 0.11 μg/g), except AS3 zircon (Duluth Complex, Minnesota), which we attribute to enrichment during hydrothermal alteration (Takehara *et al.,* 2018). All the post-Archean zircons in this study exhibit systematically low Cl contents, some of which cannot be resolved from the baseline. The average concentration is determined as 0.31 ± 0.04 μg/g.

Fluorine concentrations in all 58 Jack Hills samples are slightly higher than those in zircons from the LFB and southern Californian granitoids (2.28 ± 0.19 μg/g). Chlorine concentrations and Cl/F ratios in Jack Hills zircons appear to vary with age (Fig. 1). Significantly high Cl concentration ($[Cl]_{average}$ = 1.19 ± 0.32 μg/g) is observed in a subset of zircons within a narrow age range of 3.9–3.8 Ga. Archean grains with ages from 3.8 to 3.4 Ga display Cl contents identical to the young zircons ($[Cl]_{average}$ = 0.34 ± 0.04 μg/g), pointing to a magmatic environment with halogens levels roughly similar to modern igneous systems. Two Jack Hills zircons older than 3.9 Ga yield exceptionally high Cl contents (RSES 178-7.14 and RSES 178-8.8 with Pb-Pb ages of 4012 Ma and 4073 Ma, respectively), although the halogen measurements on the other 25 grains are within error of the range of 0.1-0.6 μg/g in the young zircons.

Halogens in Jack Hills Zircons: Primary or Secondary?

Given that mobile elements can be substituted into the zircon lattice during secondary alteration (*e.g.,* Bell *et al.,* 2016), care must be taken to ascertain that Cl and F concentrations reported for Jack Hills zircons do not represent post-crystallisation hydrothermal alteration. In our study, U-Pb ages in all Cl-rich zircons are concordant within ±10 % (Bell and Harrison, 2013) indicating little Pb loss or U gain after 3.8 Ga. In addition, two indices, including $(Sm/La)_N$ (Hoskin, 2005) and the LREE-I [= (Dy/Nd) + (Dy/Sm); Bell *et al.,* 2016], can test for possible alteration effects leading to crystalline degeneration. The high values of both indices for all grains (except one Archean zircon) are indicative of crystalline zircon, including the Cl-rich grains (see Bell *et al.,* 2016) (Fig. 2). The halogen abundances are interpreted as reflecting concentrations present during crystallisation from their primary sources magmas. The distribution of oxygen isotopes in our samples ($\delta^{18}O_{ave}$= 5.87 ± 0.17; Fig. S-7) is consistent with the prevailing populations for their corresponding time periods (Cavosie *et al.,* 2005; Trail *et al.,* 2007; Bell *et al.,* 2016) and no obvious correlation between $\delta^{18}O$ and Cl concentration is observed. The prominent excursion of Cl content in multiple 3.9–3.8 Ga zircons is higher than that seen thus far in post-Archean grains.

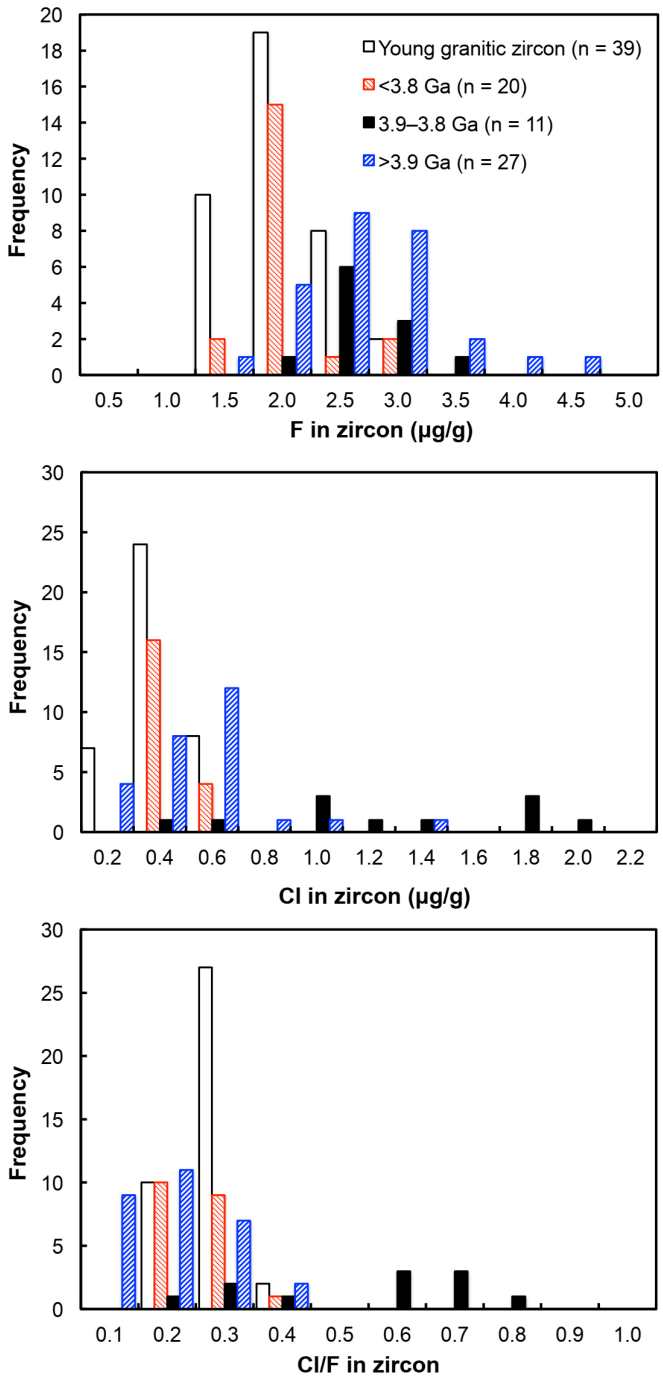

Figure 1 Fluorine concentrations in Jack Hills zircons ($[F]_{average}$ = 2.28 ± 0.19 μg/g) are generally indistinguishable from those in young granitic zircons ($[F]_{average}$ = 1.80 ± 0.11 μg/g). Elevated Cl concentrations observed in eight 3.9–3.8 Ga zircons (black columns) yield distinctly high Cl/F ratios (Cl/F > 0.3) when compared with other Jack Hills zircons.

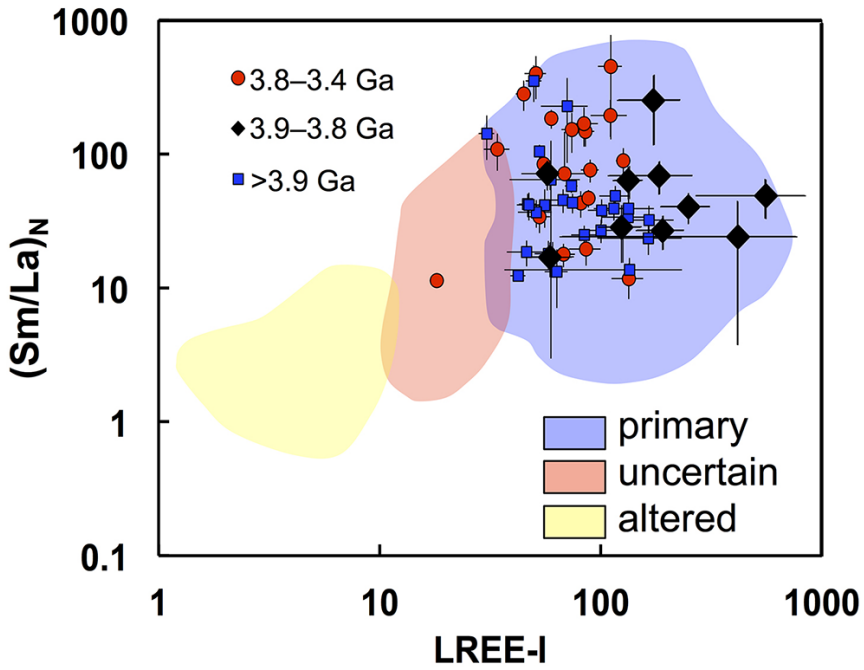

Figure 2 High values of $(Sm/La)_N$ and LREE-I [(Dy/Nd) + (Dy/Sm)] in Jack Hills sample grains imply that most of samples, especially Cl-rich zircons, are primary. The elevated Cl concentrations in zircons therefore derived from primary sources.

Group II Zircons: Recrystallisation in Cl-rich Fluids?

Bell and Harrison (2013) classified 3.9–3.8 Ga Jack Hills zircon grains into two categories. Group I exhibits temperatures and compositions similar to other igneous zircons across the age spectrum, and Group II shows high U, lower (Th/U) ratio (<0.25), and anomalously low Ti (1.82 ± 0.47 µg/g). The concordant U-Pb ages in Group II zircons and their igneous protolith similar to Group I suggest that they formed by transgressive recrystallisation, in which recrystallisation occurs across the entire zircon under high temperatures (Hoskin and Black, 2000). The distribution of halogens in the Jack Hills zircons is consistent with this classification. The *ca.* 3.9 Ga zircons in this study contain three Group I zircons ($[Cl]_{average}$ = 0.58 ± 0.28 µg/g) and eight Group II zircons ($[Cl]_{average}$ = 1.43 ± 0.33 µg/g) (Table S-2), in which two Group I zircons (RSES 56-3.17 and RSES 181-2.10) display Cl contents identical to the young zircons, and the other Group I zircon (RSES 178-20.20) has a Cl concentration higher than the young zircons, but consistent with the lowest level of Cl contents in Group II zircons (Fig. 3a).

Significant differences in Cl/F ratios are observed between Group I zircons and Group II zircons (Fig. 3b). The Jack Hills zircons with the age of 3.8–3.3 Ga and 4.2–3.9 Ga display Cl/F ratios within the range of young magmatic zircons (0.02-0.30). In addition, in the period of 3.9–3.8 Ga, no distinguishable difference of Cl/F ratios in three Group I zircons are found compared to other Jack Hills zircons. However, Cl/F ratios of Group II zircons are distinctively higher (0.33-0.74) than the ratios of young magmatic zircons.

The Ti-in-zircon crystallisation temperatures (T^{xlln}) of each Jack Hills zircon are obtained using a protocol developed in previous studies (Watson and Harrison, 2005; Harrison *et al.*, 2008). As shown in Figure 4, the Jack Hills samples group into two clusters based on their T^{xlln} and Cl/F ratios. All the Cl-rich Group II zircons exhibit distinct T^{xlln} below the nominal granite solidus (~650 °C), with an average T^{xlln} of 596 ± 17 °C. In contrast, the T^{xlln} among all other Jack Hills zircons with low Cl/F ratios overall cluster about an identical average of 680 °C, indistinguishable from the Hadean distribution (Watson and Harrison, 2005).

A possible mechanism to interpret the low Ti contents and other characteristics of Group II zircons is metamorphic transgressive recrystallisation of originally igneous zircons (Bell and Harrison, 2013). High temperature transgressive recrystallisation results in flushing the more incompatible trace elements (*e.g.*, Ce) from the mineral, an increase in compatible elements (*e.g.*, Hf, U), and homogeneous dark textures (Hoskin and Black, 2000). These characteristics are all consistent with the chemistry and internal structure of Group II zircons. Moreover, transgressive recrystallisation of zircon occurs during metamorphism at temperatures up to 600 °C. Such conditions can be achieved by the presence of hydrothermal fluids which can quickly elevate and maintain local temperatures for significant durations (Hoskin and Black, 2000). Zircon recrystallisation can occur in the contact or absence of fluids, although the elevated Cl concentrations and Cl/F ratios in Group II Jack Hills zircons relative to magmatic zircons strongly suggest the involvement of Cl-rich fluids at *ca*. 3.9 Ga, which would additionally enhance zircon recrystallisation given high solubility of ZrO_2 in saline fluids relative to pure H_2O (Bernini *et al.*, 2013).

We can roughly estimate Cl content in fluids during Group II recrystallisation based on the analysis of synthetic zircon synthesised in a Cl- and F-bearing aqueous fluid. The zircon synthesised from a fluid with 4000 µg/g Cl and 2000 µg/g F displays a Cl concentration of ~1 µg/g and a Cl/F ratio of 0.46, demonstrating that Cl can substitute into zircon when crystallising in fluid-rock systems (Table S-1). The Cl/F ratio is relatively low compared with ratios in Group II zircons, which could be attributed to the high temperature (1300 °C; 1 GPa) of the experiment relative to Hadean conditions (~680 °C) and/or the different Cl/F ratios compared to the natural fluid ratios. The partition coefficient ($D_{zircon\text{-}fluid}$) of $2.3 \pm 0.2 \times 10^{-4}$ implies fluids with Cl contents of 4×10^3-1×10^4 µg/g during Group II recrystallisation. This is similar to Cl concentrations in some brine hydrothermal fluids in the present day (*e.g.*, Stefánsson and Barnes, 2016), though significantly lower than that in modern deep crustal fluids (*e.g.*, Bodnar, 2003). Future systematic experiments are required for precise estimates on $D_{zircon\text{-}fluid}$ under different P-T conditions.

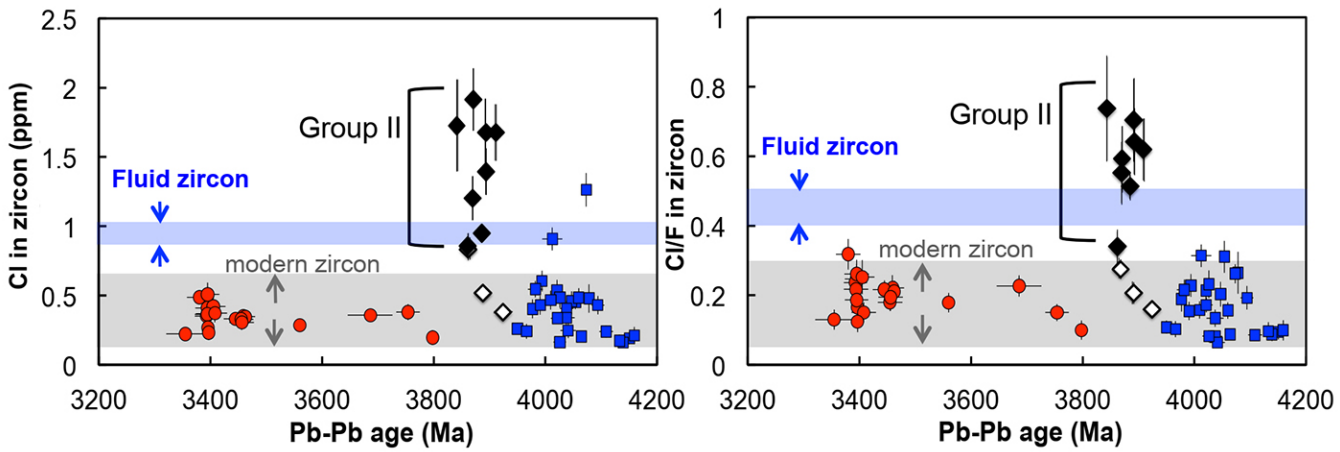

Figure 3 **(a)** Chlorine distribution and **(b)** Cl/F fractionation in Jack Hills zircons are mainly identical to the ranges determined from modern magmatic zircons in this study (red circles: <3.8 Ga zircons; white diamonds: 3.9–3.8 Ga Group I zircons; blue rectangles: >3.9 Ga zircons; grey bar: modern zircon ranges) except Group II zircons crystallised at 3.9–3.8 Ga (black diamonds). A synthetic zircon grown in an aqueous-rich fluid exhibits Cl content and Cl/F ratios (blue bars) that fall within the range of Group II.

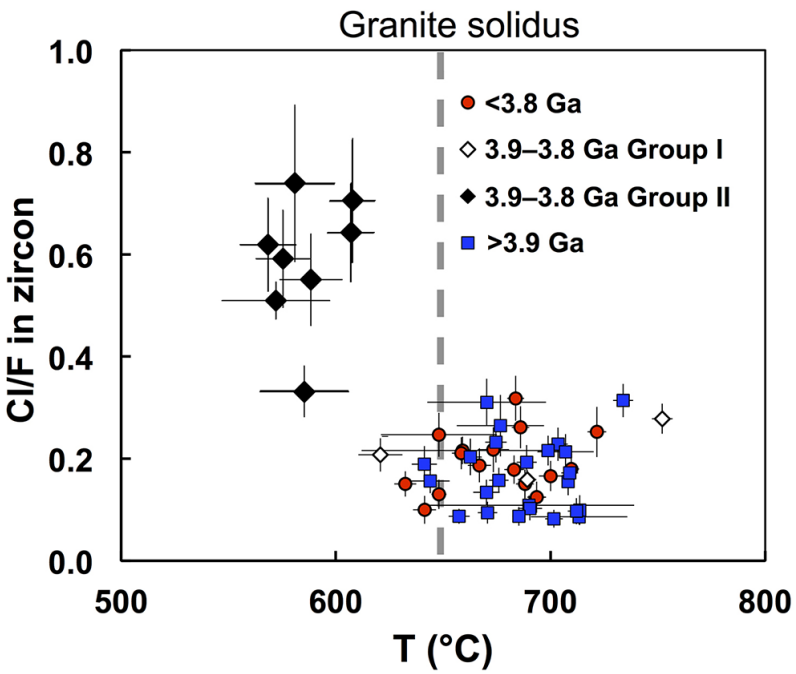

Figure 4 Chlorine-rich Group II zircons are characterised by Ti-in-zircon temperatures below granite solidus. The clearly distinguished cluster of Group II from other magmatic zircons suggests the mechanism of Group II as solid state recrystallisation involving Cl-bearing fluids.

Implications and Conclusions

Studies of Bulk Silicate Earth (BSE) halogen abundances suggest the anomalous depletions observed in volatile halogens (Cl, Br, and I) relates to their volatility during condensation from the solar nebula (Lodders, 2003; Sharp and Draper, 2013). However, these putative depletions were rendered moot by a recent analysis of the abundances of Cl, Br, and I in meteorites, which indicate much lower average abundances in primitive chondrites (Clay *et al.*, 2017) than previously thought. Given the large proportion of heavy halogens in the crustal reservoirs (80–90 % of BSE; Burgess *et al.*, 2002), notwithstanding contributions from a late veneer (*ca.* 1 % Earth mass) or complete mantle degassing (maximum estimated extraction efficiency is ~50 %; Allègre *et al.*, 1996), additional halogens transported from deep Earth would still be required, likely *via* early fluids.

The enrichment of Cl in all Group II Jack Hills zircons indicates the presence of fluids with Cl concentrations similar to modern metamorphic fluids. The average $\delta^{18}O$ identical to prevailing populations of other Jack Hills zircons suggest that rather than recycled crustal material, which would yield distinctly high $\delta^{18}O$ values, the Cl-bearing fluids occurred inside of nascent crust, either in the deeper crust or near the surface following impacts. Whether the ~3.9 Ga recrystallisation arises from meteoritic, meteoric or deep sourced fluids, the elevated Cl concentration in Group II zircons provides the first insight into halogen transfer and cycling through metamorphic fluids on early Earth.

Acknowledgements

We thank Ming-Chang Liu for assistance with our SIMS analyses and Bruce S. Brunschwig for his assistance with

the profilometer at the Molecular Materials Research Center, Caltech. Yanling Wang is also thanked for assistance. The ion microprobe facility at UCLA is partially supported by a grant from the Instrumentation and Facilities Program, Division of Earth Sciences, NSF (1339051). The research received support from EAR-1447404. We thank Veronique Le Roux, an anonymous reviewer, and the editor Horst Marschall for helpful reviews that improved the paper.

Editor: Horst R. Marschall

Additional Information

Supplementary Information accompanies this letter at http://www.geochemicalperspectivesletters.org/article1905.

Cite this letter as: Tang, H., Trail, D., Bell, E.A., Harrison, T.M. (2019) Zircon halogen geochemistry: Insights into Hadean-Archean fluids. *Geochem. Persp. Let.* 9, 49–53.

References

Allègre, C.J., Hofmann, A., O'Nions, K. (1996) The argon constraints on mantle structure. *Geophysical Research Letters* 23, 3555-3557.

Bell, E.A., Harrison, T.M. (2013) Post-Hadean transitions in Jack Hills zircon provenance: A signal of the Late Heavy Bombardment? *Earth and Planetary Science Letters* 364, 1-11.

Bell, E.A., Harrison, T.M., McCulloch, M.T., Young, E.D. (2011) Early Archean crustal evolution of the Jack Hills Zircon source terrane inferred from Lu–Hf, $^{207}Pb/^{206}Pb$, and $\delta^{18}O$ systematics of Jack Hills zircons. *Geochimica et Cosmochimica Acta* 75, 4816-4829.

Bell, E.A., Harrison, T.M., Kohl, I.E., Young, E.D. (2014) Eoarchean crustal evolution of the Jack Hills zircon source and loss of Hadean crust. *Geochimica et Cosmochimica Acta* 146, 27-42.

Bell, E.A., Boehnke, P., Harrison, T.M. (2016) Recovering the primary geochemistry of Jack Hills zircons through quantitative estimates of chemical alteration. *Geochimica et Cosmochimica Acta* 191, 187-202.

Bell, E.A., Boehnke, P., Harrison, T.M., Wielicki, M.M. (2018) Mineral inclusion assemblage and detrital zircon provenance. *Chemical Geology* 477, 151-160.

Bernini, D., Audétat, A., Dolejš, D., Keppler. H. (2013) Zircon solubility in aqueous fluids at high temperatures and pressures. *Geochimica et Cosmochimica Acta* 119, 178-187.

Bodnar, R.J. (2003) Introduction to aqueous fluid systems. In: Samson, I., Anderson, A., Marshall, D. (Eds.) *Fluid Inclusions: Analysis and Interpretation.* Mineralogical Association of Canada Short Course Series Volume 32, 81-99.

Burgess, R., Layzelle, E., Turner, G., Harris, J.W. (2002) Constraints on the age and halogen composition of mantle fluids in Siberian coated diamonds. *Earth and Planetary Science Letters* 197, 193-203.

Cavosie, A.J., Valley, J.W., Wilde, S.A. (2005) Magmatic $\delta^{18}O$ in 4400–3900 Ma detrital zircons: A record of the alteration and recycling of crust in the Early Archean. *Earth and Planetary Science Letters* 235, 663-681.

Clay, P.L., Burgess, R., Busemann, H., Ruzié-Hamilton, L., Joachim, B., Day, J.M.D., Ballentine, C.J. (2017) Halogens in chondritic meteorites and terrestrial accretion. *Nature* 551, 614-618.

Harrison, T.M., Schmitt, A.K., McCulloch, M.T., Lovera, O.M. (2008) Early (≥ 4.5 Ga) formation of terrestrial crust: Lu–Hf, $\delta^{18}O$, and Ti thermometry results for Hadean zircons. *Earth and Planetary Science Letters* 268, 476-486.

Harrison, T.M., Bell, E.A., Boehnke, P. (2017) Hadean zircon petrochronology. *Reviews in Mineralogy and Geochemistry* 83, 329-363.

Holden, P., Lanc, P., Ireland, T.R., Harrison, T.M., Foster, J.J. Bruce, Z. (2009) Mass-spectrometric mining of Hadean zircons by automated SHRIMP multi-collector and single-collector U/Pb zircon age dating: the first 100,000 grains. *International Journal of Mass Spectrometry* 286, 53-63.

Hoskin P.W.O. (2005) Trace-element composition of hydrothermal zircon and the alteration of Hadean zircon from the Jack Hills, Australia. *Geochimica et Cosmochimica Acta* 69, 637–648.

Hoskin, P.W.O., Black, L.P. (2000) Metamorphic zircon formation by solid-state recrystallization of protolith igneous zircon. *Journal of metamorphic Geology* 18, 423-439.

Lodders, K. (2003) Solar system abundances and condensation temperatures of the elements. *The Astrophysical Journal* 591, 1220-1247.

Manning, C.E., Mojzsis, S.J., Harrison, T.M. (2006) Geology, age and origin of supracrustal rocks at Akilia, West Greenland. *American Journal of Science* 306, 303-366.

Mojzsis, S.J., Harrison, T.M., Pidgeon, R.T. (2001) Oxygen-isotope evidence from ancient zircons for liquid water at the Earth's surface 4,300 Myr ago. *Nature* 409, 178-181.

O'Neil, J., Carlson, R.W., Francis, D., Stevenson, R.K. (2008) Neodymium-142 evidence for Hadean mafic crust. *Science* 321, 1828-1831.

Peck, W.H., Valley, J.W., Wilde, S.A., Graham, C.M. (2001) Oxygen isotope ratios and rare earth elements in 3.3 to 4.4 Ga zircons: Ion microprobe evidence for high $\delta^{18}O$ continental crust and oceans in the Early Archean. *Geochimica et Cosmochimica Acta* 65, 4215-4229.

Sharp, Z.D., Draper, D.S. (2013) The chlorine abundance of Earth: implications for a habitable planet. *Earth and Planetary Science Letters* 369, 71-77.

Stefánsson, A., Barnes, J.D. (2016) Chlorine isotope geochemistry of Icelandic thermal fluids: Implications for geothermal system behavior at divergent plate boundaries. *Earth and Planetary Science Letters* 449, 69-78.

Takehara, M., Horie, K., Hokada, T., Kiyokawa, S. (2018) New insight into disturbance of U-Pb and trace-element systems in hydrothermally altered zircon via SHRIMP analyses of zircon from the Duluth Gabbro. *Chemical Geology* 484, 168-178.

Trail, D., Mojzsis, S.J., Harrison, T.M., Schmitt, A.K., Watson, E.B., Young, E.D. (2007) Constraints on Hadean zircon protoliths from oxygen isotopes, Ti-thermometry, and rare earth elements. *Geochemistry, Geophysics, Geosystems* 8, 1-22.

Trail, D., Watson, E.B., Tailby, N.D. (2011) The oxidation state of Hadean magmas and implications for early Earth's atmosphere. *Nature* 480, 79-82.

Trail. D., Cherniak, D.J., Watson, E.B., Harrison, T.M., Weiss, B.P., Szumila., I. (2016) Li zoning in zircon as a potential geospeedometer and peak temperature indicator. *Contributions to Mineralogy and Petrology* 171, 25-40.

Watson, E.B., Harrison, T.M. (2005) Zircon thermometer reveals minimum melting conditions on earliest Earth. *Science* 308, 841-844.

Geochemical Perspectives Letters

Zircon halogen geochemistry: Insights into Hadean-Archean fluids

H. Tang, D. Trail, E. A. Bell, T. M. Harrison

Supplementary Information

The Supplementary Information includes:

- Sample Description
- Analytical Method
- REE Pattern in Jack Hills Zircons
- Oxygen Isotope Compositions
- Figures S-1 to S-8
- Tables S-1 to S-4
- Supplementary Information References

Sample Description

1. Jack Hills Zircon

Zircons are extracted from *ca.* 3 Ga Jack Hills (JH) metaconglomerates, Western Australia (Spaggiari *et al.*, 2007; Holden *et al.*, 2009). Numerous age studies of JH detrital zircons show a characteristic bimodal distribution with peaks close to 4.1 Ga and 3.4 Ga (Compston and Pidgeon 1986; Maas *et al.*, 1992; Amelin 1998; Amelin *et al.*, 1999; Mojzsis *et al.*, 2001; Cavoise *et al.*, 2004; Trail *et al.*, 2007; Holden *et al.*, 2009; Bell *et al.*, 2011, 2014; Bell and Harrison, 2013). The JH zircons in our studies display U-Pb ages from 4.2 to 3.4 Ga. Oxygen isotope ratios and REE patterns in some of grains have been investigated in previous studies, implying that all samples preserve the primary magmatic information without late alteration after crystallization (Bell *et al.*, 2011; Bell and Harrison, 2013; Bell *et al.*, 2014, 2016).

The characteristics of Group I and group II zircons were first illustrated in Bell and Harrison (2013). Here we show backscatter images (BSE) and cathodoluminescence images (CL) of representative Group I and Group II Jack Hills zircons in Figure S-1. Note that Group I zircons show original oscillatory zonation or cloudy zonation (Fig. S-1a), whereas Group II zircons are dark homogeneous without zonation in CL (Fig. S-1b).

2. Lachlan Fold Belt and California Arc

Lachlan Fold Belt (LFB) contains over 400 different granitoid plutons with ages spanning from 420 to 390 Ma (White and Chappell, 1983; Chappell and Simpson, 1984). The geochemical differences of zircons from diverse parent rocks of LFB have been widely investigated due to the well-studied geologic and tectonic history of LFB.

We selected granitoids from the LFB studied investigated by Trail *et al.* (2017). Four metaluminous rocks (ASI<1) and six peraluminous rocks (ASI>1) were sampled from LFB. The metaluminous rocks include Tara, Jindabyne, Buckleys Lake, and Glenbog (Griffin *et al.*, 1978; Hine *et al.*, 1978; Chappell *et al.*, 1990), all of which were classified as I-type rocks (Chappell, 1974). The peraluminous rocks include Cootalantra, Bullenbalong, Dalgety, Cowra, Shannons Flats, and Longwood (Joyce, 1973; Hine *et al.*, 1978; Chappell *et al.*, 1990, 1993; Phillips *et al.*, 1981). Longwood is a leucocratic 2-mica granite located in the Strathbogie Range, Southern Australia (Bell *et al.*, 2017). The whole rock ASI values of peraluminous samples range from 1.06 to 1.28.

The Peninsular ranges batholith of southern California and Baja California are divided into a western predominantly magnetite-bearing plutonic subprovince and an eastern magnetite-free plutonic subprovince, which define a west-to-east transect across southern San Diego County. The granitic plutons along this transect show systematically distinctive geophysical, geobarometric, mineralogical, geochemical, and isotopic characteristics, although U-Pb ages in zircon grains suggest an approximately similar crystallisation age of *ca.* 100 Ma. The $\delta^{18}O$ value varied from the low "normal" igneous $\delta^{18}O$ values (+6 to +8.5) in the western zone to the higher values (+9 to +12) in the eastern zone (Silver *et al.*, 1979). Besides, the magnetite/ilmenite distinction indicates a variation of oxygen fugacity in the magma during progressive crystallisation (Todd *et al.*, 2003 and reference within). Magmas in the west of this margin interacted with oceanic crust and crystallised magnetite ± ilmenite, whereas those in the east intruded reduced (low Fe^{3+}/Fe) crust and thus crystallised ilmenite and hardly any magnetite. Here we selected zircons separated from a peraluminous ilmenite-bearing granite (ASI=1.03) from the San Jacinto Mountains in the eastern PRB (IG4) to obtain the halogen abundance as an analog for Jack Hills detrital zircons.

Sample BB12 is a metaluminous magnetite series granitoid (ASI=0.91) sampled from the Cretaceous Cactus Flat quartz diorite (*e.g.*, Barth *et al.*, 2016), a satellite pluton of the Big Bear Intrusive Complex (BBIC) in the San Bernardino Mountains of southern California. The BBIC and satellite plutons also formed during the Cretaceous subduction episode that yielded the PRB.

3. Synthetic Zircons

Zircons were synthesised under two conditions at the University of Rochester. The zircon grain for determination of the ion microprobe detection limit is grown following the method described in Trail *et al.* (2016). The experimental technique is known as the flux method (*e.g.*, Chase and Osmer, 1966; Suzuki *et al.*, 1992; Hanchar *et al.*, 2001). The starting material is consisted of a mixture of MoO_3-Li_2CO_3-$ZrSiO_4$ in a ratio of 1:0.18:0.06 by weight. The starting mixtures are firmly packed into Pt crucibles, suspended, and soaked in a furnace at 1×10^5 Pa, 1400°C for 3 hours. The sample is then cooled to ~900°C at 3°C/hr. Zircons synthesised by this method are expected to be free of volatile Cl and F. Thus the halogen abundances determined in these zircons are interpreted to be the detection limits of the *in situ* analysis.

We also synthesised zircon grains in the ZrO_2-SiO_2-H_2O-CaO-F-Cl system. Fluid concentrations of 2000 μg/g and 4000 μg/g for F and Cl, respectively were targeted. The mixtures are sealed into Pt capsules and placed in the piston cylinder at 1300°C, 1 GPa for 72 hours. Zircons grown in the halogen-rich fluid system are analysed as an analogue of recrystallised zircon to test if Cl and F can be substituted into zircon lattice.

Analytical Method

Zircons were hand picked from mineral separates after crushing the rock samples and separating high-density minerals using heavy liquid. Grains were mounted in epoxy and polished to 1 μm using SiC abrasive papers. Then sample mounts were gold-coated for *in situ* analyses.

The *in situ* analyses were performed on SIMS 1290 at UCLA. We developed a new analytical procedure to quantify the trace abundance of volatile elements in zircon. Great care has been taken to prevent contamination from the "gardening effect" (i.e., reworking of surface contamination into the sample volume) and to characterise appropriate standards with which to measure the relative sensitivity factor (RSF). The RSF is defined as the scaling factor that multiplies measured ion ratios to derive the true ratios of corresponding ion species. In this regard, the RSF of element x in zircon can be defined as the following equation,

$$RSF_{X/Si} = \frac{{}^{C}{}_{i_X}/{}^{C}{}_{j_{Si}}}{{}^{I}{}_{i_X}/{}^{I}{}_{j_{Si}}} \qquad \text{(Eq. S-1)}$$

where the subscripts ${}^{i}X$ and ${}^{j}Si$ denote measured species of volatile species of interest X and Si, respectively, C and I indicate the true concentration and measured signal intensity on SIMS. RSF must be measured under the same conditions as the unknowns. To avoid any analytical artifact, the standard is required to be homogeneous on species of interest and matrix-matched with the unknowns. For major elements (*e.g.*, Si), concentrations can be determined by electron microprobe methods. However, this method cannot be applied to trace elements due to the detection limits. To obtain the proper standard with known and homogeneous volatile species, we implanted two zircon mounts with known fluences of F or Cl as standards in preparation for SIMS depth

profiling (Zinner and Walker, 1975; Leta and Morrison, 1980; Burnett *et al.*, 2015; Steele *et al.*, 2017).

We selected ^{19}F and ^{37}Cl as implanted species. Except ^{19}F as the only nuclide of F, ^{37}Cl are the implanted isotope due to the lower background compared to ^{35}Cl in zircon. The similar RSF also makes it appropriate. The optimised implantation energy is estimated by simulating implanted ion distribution using the SRIM code (Ziegler, 2004). Accordingly, the energy values of ^{19}F and ^{37}Cl implantation are set to be 100 keV and 190 keV, respectively, corresponding to the expected implant peaks appearing in ~170 nm and ~140 nm from the surface of zircon (Fig. S-2). The nominal implanted fluence of ^{19}F and ^{37}Cl is 1×10^{14} cm^{-2}. Two Mud Tank zircon mounts were prepared for the individual implantation of ^{19}F and ^{37}Cl by a rastered beam at CuttingEdge Ions, Anaheim, California. The uncertainty of fluence is estimated to be ±10 % (communication with CuttingEdge Ions).

The implanted samples were analysed on the CAMECA *ims* 1290 ion microprobe at UCLA. Depth profiles were obtained in Mud Tank zircon mounts to estimate RSF. The implanted samples were sputtered with a 10 keV Cs^+ primary ion beam. The primary beam current was ~2 nA, rastered over a 50 μm × 50 μm area. A rectangular field aperture was applied to restrict transmitted ions to the center 10 μm × 10 μm area to get rid of any sidewall effect. Negative secondary ions were collected with the axial electron multiplier (EM) in peak jumping (mono-collection) mode with the mass sequence of 18.5, $^{19}F^-$, $^{30}Si^-$, $^{31}P^-$, $^{35}Cl^-$, and $^{37}Cl^-$. A mass resolving power of 6,000 was used to resolve interferences from the peaks of interest. The noise in the ion counting system is less than 10^{-3} counts per second (cps), and data were corrected for a dead time of 60 ns. In addition, natural zircons were measured following the same procedure described above.

The implanted standards were sputtered through the peak of the profile until the signal decayed to a stable background (~1 hour). According to Steele *et al.* (2017), the RSF of elements of interest relative to silicon in zircon can be determined using the following equation,

$$RSF\left(\frac{X}{^{30}Si}\right) = \frac{I_{^{30}Si}F_X t}{C_{^{30}Si}DA_X} \qquad \text{(Eq. S-2)}$$

where $C_{^{30}Si}$ is calculated based on the density and molar mass of zircon, $I_{^{30}Si}$ is the intensity of ^{30}Si, A_X is the integrated counts of implanted element of interest throughout the entire depth profile, and t is the time of the entire analysis. D is the total depth of the analysis which was estimated by using a Bruker DektakXT stylus profilometer at the Molecular Materials Research Center, Caltech. In this study, the RSF was measured once every day to confirm the stability of the instrument. The average values of the RSF were thereby determined to be 0.0366±0.0017 for F and 0.0331±0.0018 for Cl.

Figure S-2 shows an example of the depth profiling of ^{37}Cl implanted Mud Tank zircon. The implanted ^{37}Cl was calculated by subtracting background ^{37}Cl from the measured ^{37}Cl count rate, in which the background ^{37}Cl was proportionally estimated from ^{35}Cl count rate. Regarding the background and surface contamination of ^{19}F in zircon, we estimated ^{19}F background by averaging ^{19}F count rate after 2,300s since no implanted element (F or Cl) can be detected after 2,300s. The surface contamination of ^{19}F cannot to eliminated by measuring its isotope. Thus, we collected the profile from the maximum ^{19}F count rate and simulated a half of the depth profile assuming that the implanted ^{19}F was normally distributed on the depth (Fig. S-3). Depth profiles of natural zircon samples were analysed on SIMS with the same approach. To avoid any potential surface contamination caused by the gardening effect, we only select the data collected after 2,300 s for data reduction (e.g., Fig S-4). The halogen content can be calculated using the following equation,

$$[X]/(\mu g/g) = RSF \times I_{avg}^{X/30Si} \times C(^{30}Si)_{zrn} \times 10^6/R_X \qquad \text{(Eq. S-3)}$$

and the uncertainty was propagated using:

$$\sigma[[X]/(\mu g/g)] = \sqrt{\left(\frac{\sigma_{RSF}}{RSF}\right)^2 + \left(\frac{\sigma_{I^{X/30Si}}}{I_{avg}^{X/30Si}}\right)^2} \times [X]/(\mu g/g) \qquad \text{(Eq. S-4).}$$

In these equations, $\sigma_{I^{X/30Si}}$ represents the standard deviation of the average I_X/I_{30Si} ratio, σ_{RSF} is the uncertainty from RSF, $C(^{30}Si)_{zrn}$ represents ^{30}Si content in zircon (0.51wt%), and R_X is the relative abundance of ^{19}F or ^{35}Cl in the corresponding elements (we assume that $RSF_{Cl/Si} = RSF_{37Cl/30Si} = RSF_{35Cl/30Si}$).

We determined the detection limit of F and Cl by measuring synthetic zircons which were grown under volatile-free conditions. The synthetic zircons display the lowest F and Cl concentrations, which are conservatively assumed to be our baseline values for F and Cl. As shown in Figure S-5, the baseline values decrease slightly from day 1 to day 2 and become indistinguishable from day 2, after which the measurement of unknown zircons started. The baseline values of F and Cl were thereby determined to be 0.78±0.07 μg/g and 0.12±0.02 μg/g, respectively.

The presence of cracks and inclusions can significantly result in the overestimated halogen abundances. Thus, we carefully identified any cracks/inclusions in SEM at high magnification and only selected the data for which no crack or inclusion was found. Representative BSE and secondary electron images are shown in Figure S-6.

REE Pattern in Jack Hills Zircons

Trace elements (including REE, Hf, Th and U) were targeted in our study to search for geochemical differences resulting from water-rock interaction, oxygen fugacity, and possible late alteration processes. Figure S-7 shows chondrite-normalised REE results for all 58 Jack Hills zircons. Some of the data are referred to Bell and Harrison (2013), Bell *et al.* (2014), and Bell *et al.* (2016). All zircons show the low LREE/HREE, positive Ce anomalies, and negative Eu anomalies consistent to most terrestrial zircons. All REE patterns are plotted into the zone of primary zircon defined in Bell *et al.* (2016).

Oxygen Isotope Compositions

Figure S-8 shows $\delta^{18}O$ results for Jack Hills zircon samples in this study. In general, the $\delta^{18}O$ distribution in our measurement is consistent with the prevailing population at the corresponding time periods (Trail *et al.*, 2007; Cavosie *et al.*, 2005; Bell *et al.*, 2016). The average $\delta^{18}O$ values of zircons with age ranges of 3.8–3.3 Ga, 3.9–3.8 Ga, and 4.2–3.9 Ga are estimated to be 5.55 ± 0.15 ‰, 5.91 ± 0.48 ‰, and 6.06 ± 0.26 ‰, respectively.

Supplementary Figures

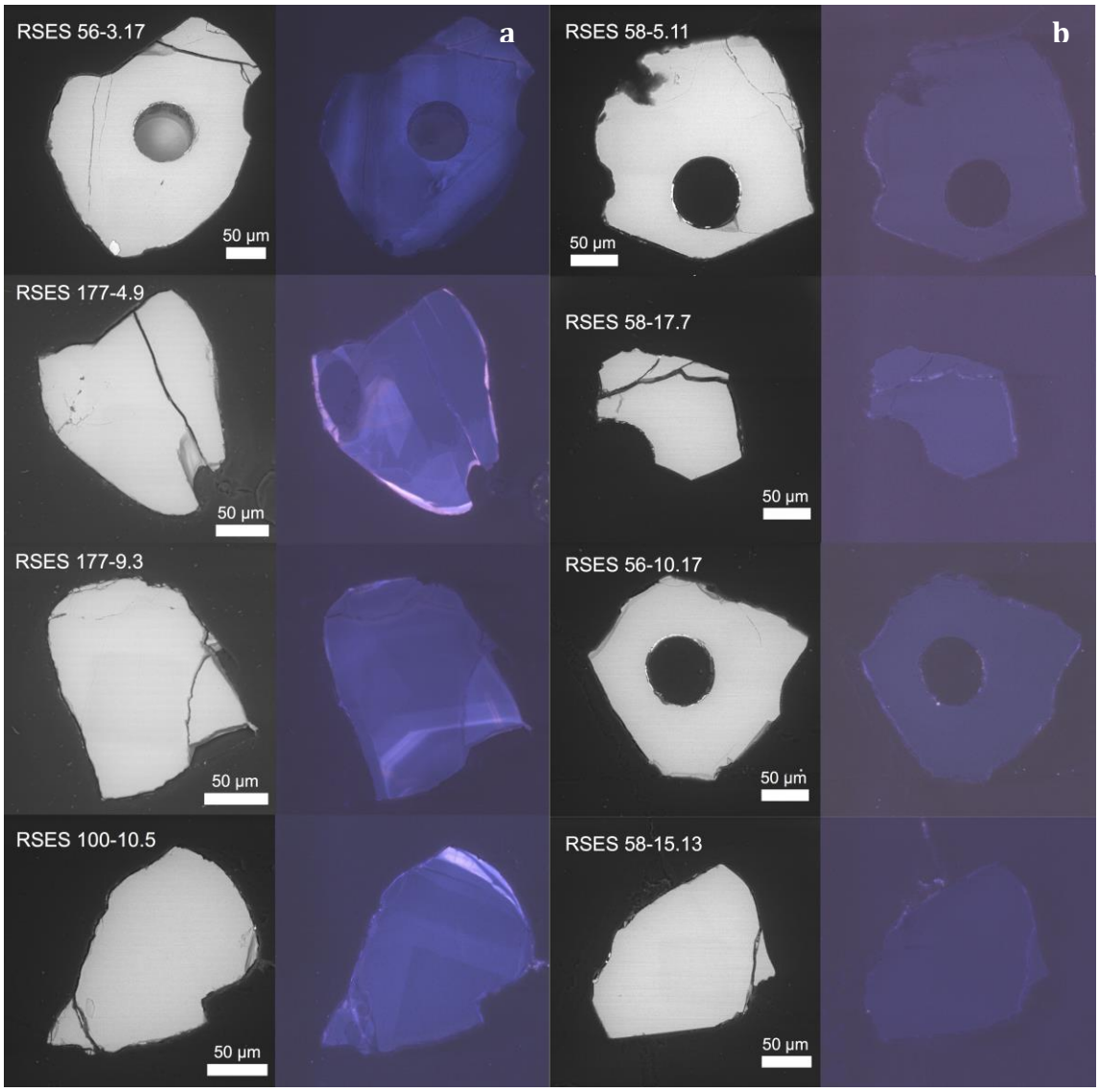

Figure S-1 (a) Backscatter and cathodoluminescence images of representative Group I zircons; **(b)** backscatter and cathodoluminescence images of representative Group II zircons.

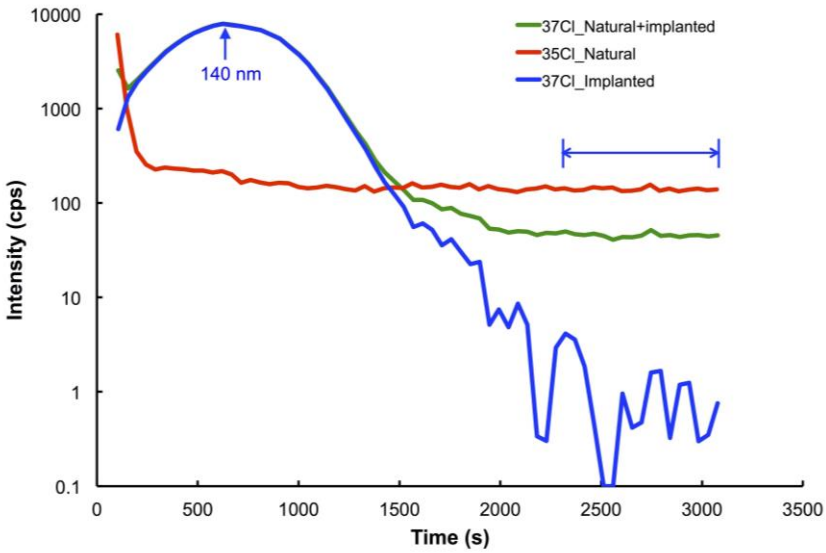

Figure S-2 Plots showing a characteristic ^{37}Cl implanted profile measured in Mud Tank zircon, the count rate of implanted ^{37}Cl (blue line) is proportionally calculated by ^{35}Cl intensity (red line).

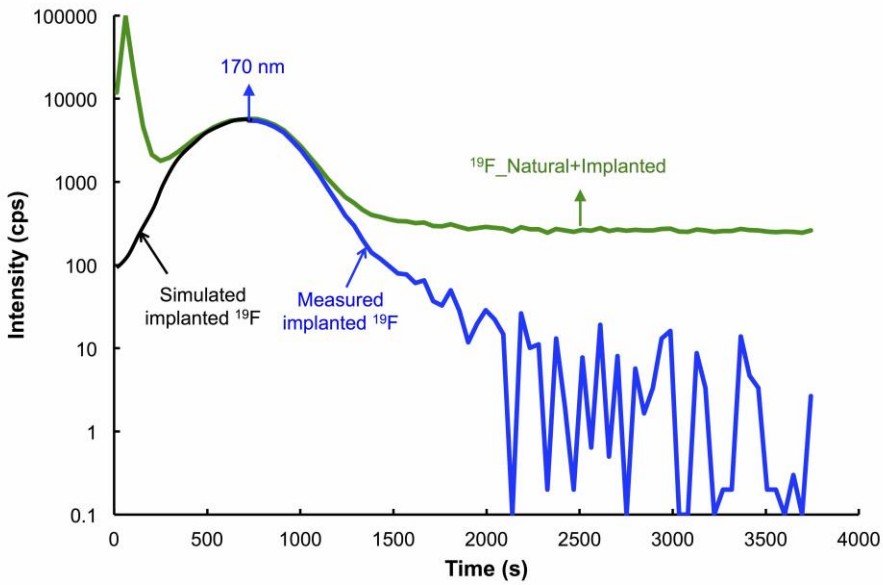

Figure S-3 Plots showing a characteristic ^{19}F implanted profile measured in Mud Tank zircon, the implanted ^{19}F counts are accounted from the maximum ^{19}F count rate (blue line) and simulation of a half of depth profile (black line) assuming normal distribution of implanted ^{19}F on the depth.

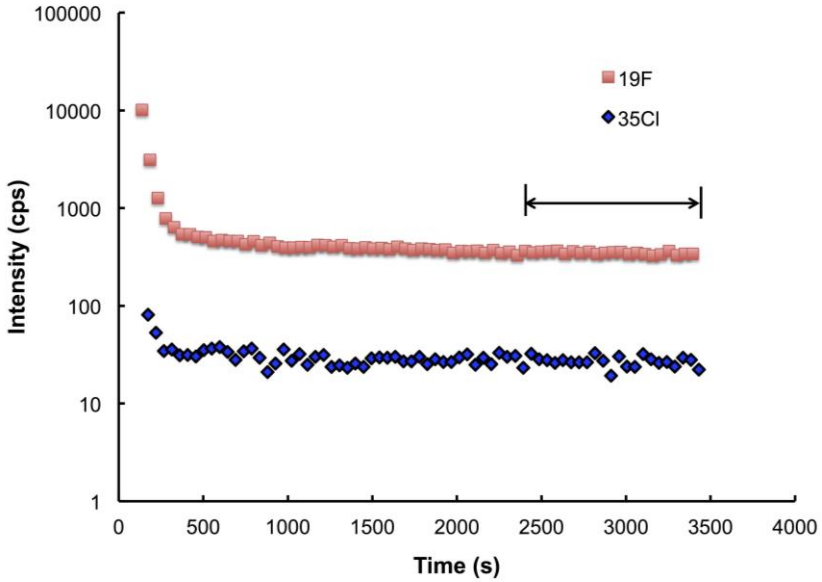

Figure S-4 A plot of ^{19}F and ^{35}Cl count rates with analytical time in a Jack Hills zircon. The data collected after 2,300 s are used to estimate F and Cl concentration in zircons.

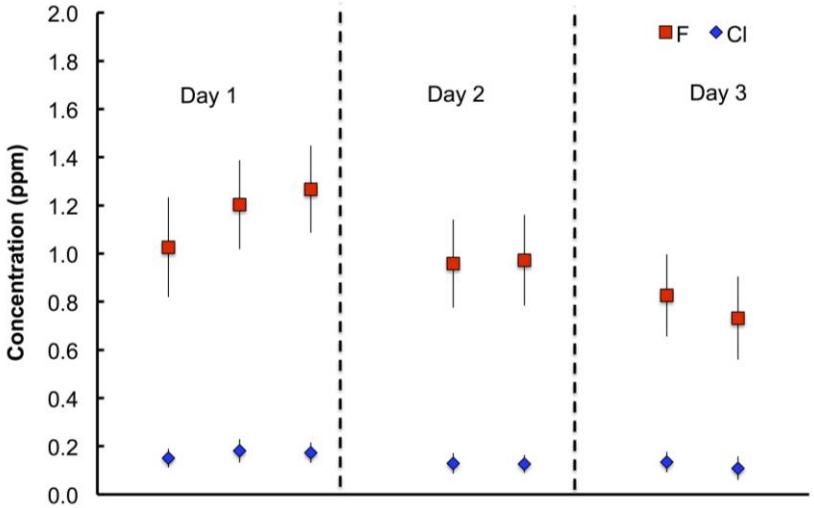

Figure S-5 F and Cl concentrations in three days determined from a synthetic zircon grown from volatile-free conditions. The detection limits are calculated from the average of the concentrations in Day 2 and Day 3.

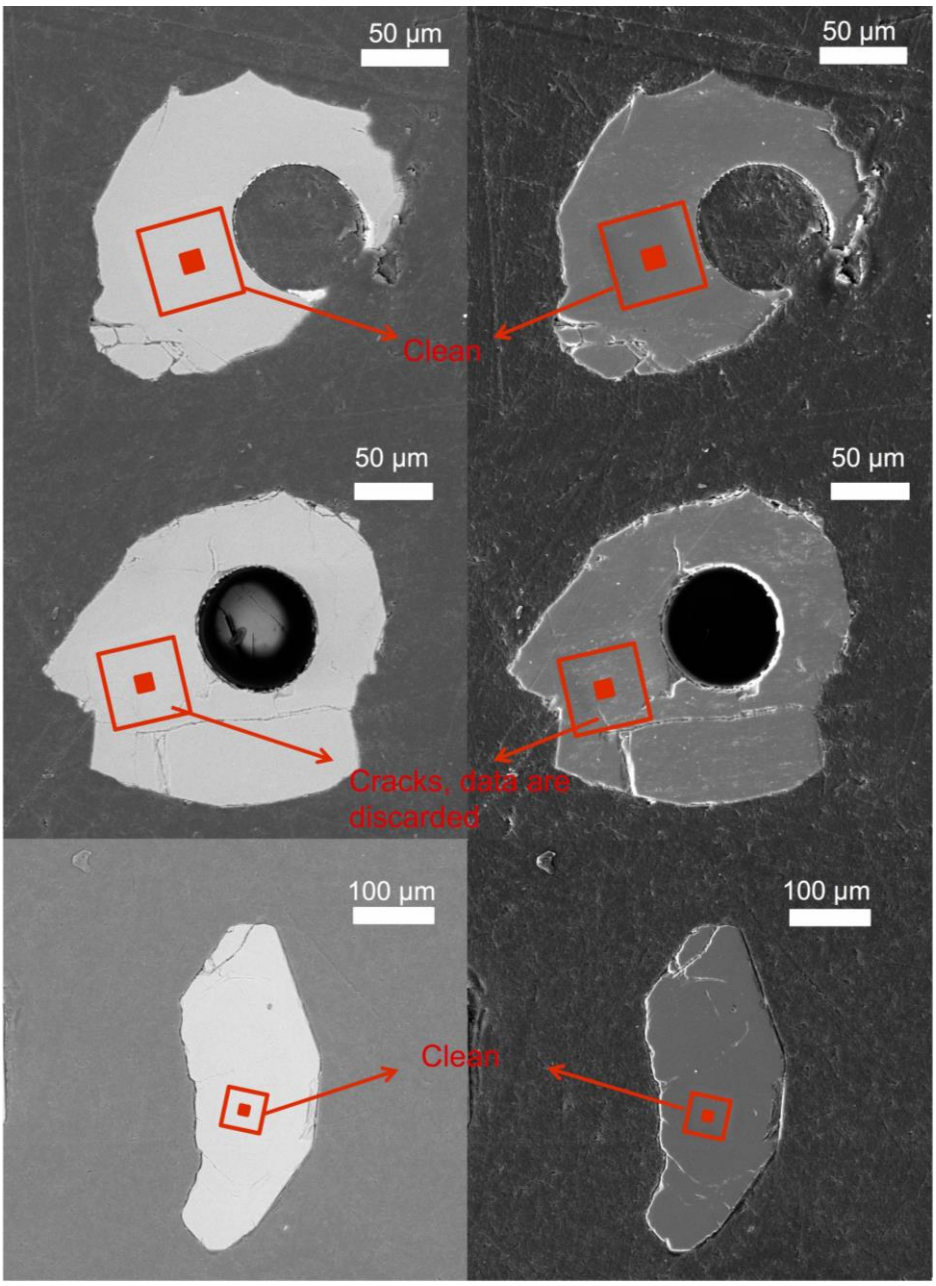

Figure S-6 BSE and SE images of representative samples. The open red rectangles indicate 50 µm × 50 µm raster areas and the solid red rectangles represent 10 µm × 10 µm detection areas. Data were discarded in the case of any presence of cracks or inclusions inside of raster areas.

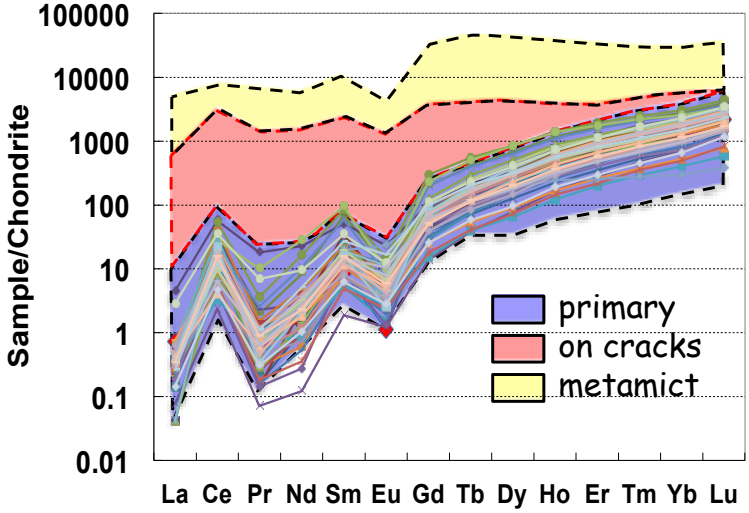

Figure S-7 REE patterns in all Jack Hills zircon samples.

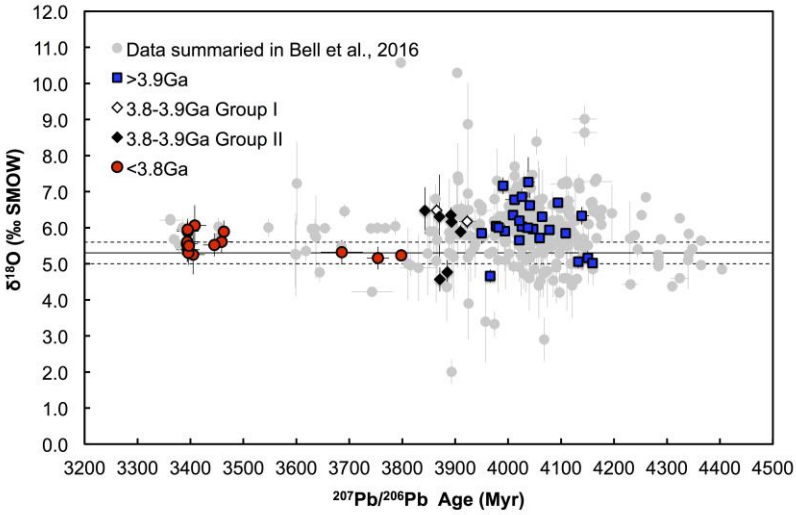

Figure S-8 Oxygen isotope compositions plotted with Pb-Pb ages in Jack Hills zircon samples.

Supplementary Tables

Table S-1 Halogen in modern zircon samples.

Sample ID	ASI		ASI citation	F (μg/g)	2 s.e.	Cl (μg/g)	2 s.e.	Cl/F	2 s.e.
Synthetic zircon									
SynZr@2		Day1		1.03	0.21	0.15	0.04	0.15	0.05
SynZr1_mt2@1		Day1		1.20	0.18	0.18	0.05	0.15	0.05
SynZr2_mt2@1		Day1		1.27	0.18	0.17	0.04	0.14	0.04
SynZr@3		Day2		0.96	0.18	0.13	0.04	0.13	0.05
SynZr1_mt2@2		Day2		0.97	0.19	0.13	0.04	0.13	0.05
SynZr1_mt2@3		Day3		0.83	0.17	0.13	0.04	0.16	0.06
SynZr2_mt2@2		Day3		0.73	0.17	0.11	0.05	0.15	0.08
Baseline				0.78	0.07	0.12	0.02		
fluid zircon				2.07	0.10	0.90	0.08	0.44	0.05
Geostandard									
AS3@1				3.06	0.31	0.30	0.05	0.10	0.02
AS3@2				10.60	1.02	0.22	0.04	0.02	0.00
AS3@4				18.18	0.52	0.41	0.07	0.02	0.00
AS3@5				8.86	0.33	0.39	0.04	0.04	0.00
91500@1				1.70	0.08	0.28	0.05	0.16	0.03
91500@2				1.71	0.13	0.28	0.08	0.16	0.05
		Location							
Peninsular range I-type zircon									
BB12@1	0.91	Cretaceous Cactus Flat	this study	1.80	0.16	0.29	0.06	0.16	0.04
BB12@2	0.91	Cretaceous Cactus Flat	this study	2.45	0.13	0.27	0.06	0.11	0.03
BB12@3	0.91	Cretaceous Cactus Flat	this study	2.49	0.12	0.28	0.06	0.11	0.03
BB12@4	0.91	Cretaceous Cactus Flat	this study	2.53	0.18	0.28	0.04	0.11	0.02
BB12@5	0.91	Cretaceous Cactus Flat	this study	2.07	0.19	0.27	0.05	0.13	0.03
BB12@6	0.91	Cretaceous Cactus Flat	this study	2.00	0.14	0.25	0.05	0.13	0.03
IG4m@1	1.03	San Jacinto Mountains	this study	1.79	0.12	0.36	0.06	0.20	0.04
Lachlan Fold Belt I-type zircon									
W59@3	0.98	Tara	Trail *et al.*, 2017	1.47	0.11	0.17	0.04	0.12	0.03
W59@10	0.98	Tara	Trail *et al.*, 2017	1.43	0.13	0.17	0.04	0.12	0.03
W59@5	0.98	Tara	Trail *et al.*, 2017	1.68	0.09	0.14	0.03	0.08	0.02
W61@9	0.98	Jinbabyne	Trail *et al.*, 2017	1.44	0.12	0.21	0.04	0.15	0.03
W61@4	0.98	Jinbabyne	Trail *et al.*, 2017	1.52	0.12	0.16	0.03	0.10	0.02
W61@1	0.98	Jinbabyne	Trail *et al.*, 2017	1.49	0.12	0.17	0.04	0.12	0.03
W66@2	0.99	Buckleys Lake	Trail *et al.*, 2017	1.48	0.12	0.20	0.03	0.13	0.02
W66@5	0.99	Buckleys Lake	Trail *et al.*, 2017	1.45	0.11	0.19	0.04	0.13	0.03
W66@8	0.99	Buckleys Lake	Trail *et al.*, 2017	1.43	0.15	0.21	0.05	0.15	0.04
W66@10	0.99	Buckleys Lake	Trail *et al.*, 2017	1.47	0.16	0.20	0.03	0.14	0.03
W67@8	0.94	Glenbog	Trail *et al.*, 2017	1.49	0.21	0.19	0.04	0.13	0.03
Lachlan Fold Belt S-type zircon									
W58@3	1.16	Cootralantra	Trail *et al.*, 2017	1.59	0.12	0.32	0.04	0.20	0.03
W58@6	1.16	Cootralantra	Trail *et al.*, 2017	2.07	0.11	0.32	0.04	0.16	0.02
W58@7	1.16	Cootralantra	Trail *et al.*, 2017	1.62	0.13	0.45	0.08	0.28	0.05
W58@9	1.16	Cootralantra	Trail *et al.*, 2017	1.70	0.11	0.39	0.05	0.23	0.03
W58@10	1.16	Cootralantra	Trail *et al.*, 2017	1.70	0.13	0.24	0.05	0.14	0.03

W60@5	1.18	Bullenbalong	Trail *et al.*, 2017	2.14	0.14	0.26	0.05	0.12	0.03
W60@8	1.18	Bullenbalong	Trail *et al.*, 2017	1.62	0.19	0.36	0.05	0.22	0.04
W60@9	1.18	Bullenbalong	Trail *et al.*, 2017	2.54	0.39	0.35	0.04	0.14	0.03
W74@9	1.03	Shannons Flat	Trail *et al.*, 2017	1.83	0.07	0.30	0.04	0.17	0.02
W183@7	1.27	Cowra	Trail *et al.*, 2017	1.90	0.17	0.27	0.06	0.14	0.03
W183@9	1.27	Cowra	Trail *et al.*, 2017	1.65	0.14	0.34	0.05	0.20	0.03
W183@10	1.27	Cowra	Trail *et al.*, 2017	1.66	0.17	0.46	0.06	0.28	0.04
W64@1	1.06	Dalgety	Trail *et al.*, 2017	1.70	0.14	0.42	0.03	0.25	0.03
W64@10	1.06	Dalgety	Trail *et al.*, 2017	2.15	0.11	0.28	0.04	0.13	0.02
W64@10	1.06	Dalgety	Trail *et al.*, 2017	1.65	0.18	0.39	0.06	0.24	0.04
Strathbogie Range									
SR@1	1.28	Longwood	Phillips *et al.*, 1981	2.30	0.15	0.56	0.07	0.25	0.04
SR@2	1.28	Longwood	Phillips *et al.*, 1981	1.60	0.17	0.48	0.06	0.30	0.05
SR@3	1.28	Longwood	Phillips *et al.*, 1981	1.46	0.15	0.44	0.07	0.30	0.06
SR@4	1.28	Longwood	Phillips *et al.*, 1981	1.67	0.17	0.40	0.06	0.24	0.05
SR@5	1.28	Longwood	Phillips *et al.*, 1981	1.78	0.17	0.39	0.07	0.22	0.05
SR@6	1.28	Longwood	Phillips *et al.*, 1981	2.49	0.15	0.58	0.09	0.23	0.04
Average				**1.80**		**0.31**		**0.17**	
2 s.e.				**0.11**		**0.04**		**0.02**	

Table S-2 Halogen in Jack Hills zircons.

Jack Hills Sample	Pb-Pb age (Ma)	2 s.e.	Age citation	F (μg/g)	2 s.e.	Cl (μg/g)	2 s.e.	Cl/F	2 s.e.
<3.8 Ga									
RSES 51-4.2	3686	40	Bell *et al.*, 2011	1.58	0.10	0.36	0.04	0.23	0.03
RSES 51-5.4	3459	21	Bell *et al.*, 2011	1.57	0.13	0.35	0.05	0.22	0.04
RSES 51-5.7	3395	21	Bell *et al.*, 2011	1.49	0.09	0.37	0.06	0.25	0.04
RSES 51-6.2	3445	21	Bell *et al.*, 2011	1.53	0.10	0.33	0.03	0.22	0.03
RSES 51-6.9	3393	21	Bell *et al.*, 2011	1.49	0.13	0.35	0.03	0.24	0.03
RSES 51-10.10	3463	3	Bell *et al.*, 2011	1.63	0.08	0.34	0.05	0.21	0.03
RSES 51-10.11	3395	22	Bell *et al.*, 2011	1.57	0.14	0.41	0.05	0.26	0.04
RSES 51-10.14	3380	22	Bell *et al.*, 2011	1.53	0.17	0.49	0.04	0.32	0.04
RSES 51-12.1	3455	22	Bell *et al.*, 2011	1.82	0.12	0.33	0.04	0.18	0.03
RSES 51-12.9	3405	22	Bell *et al.*, 2011	1.67	0.10	0.42	0.08	0.25	0.05
RSES 51-12.13	3394	22	Bell *et al.*, 2011	1.67	0.17	0.36	0.06	0.22	0.04
RSES 51-13.5	3456	22	Bell *et al.*, 2011	1.57	0.15	0.31	0.05	0.19	0.04
RSES 51-14.3	3560	3	Bell *et al.*, 2011	1.60	0.08	0.29	0.04	0.18	0.03
RSES 51-16.3	3396	3	Bell *et al.*, 2011	1.62	0.13	0.27	0.04	0.17	0.03
RSES 51-4.7	3754	21	Bell *et al.*, 2011	2.53	0.15	0.38	0.06	0.15	0.02
RSES 51-11.1	3408	22	Bell *et al.*, 2011	2.48	0.17	0.37	0.07	0.15	0.03
RSES 51-16.1	3397	2	Bell *et al.*, 2011	1.87	0.13	0.23	0.05	0.12	0.03
RSES 51-4.1	3395	21	Bell *et al.*, 2011	2.72	0.18	0.51	0.08	0.19	0.03
RSES 195-1.15	3355	34	Holden *et al.*, 2009	1.71	0.16	0.22	0.04	0.13	0.03
RSES 181-5-2	3798	11.0	Holden *et al.*, 2009	1.97	0.11	0.20	0.05	0.10	0.03
3.9−3.8 Ga									
Group I									
RSES 178-20.20	3865	10.2	Holden *et al.*, 2009	3.02	0.13	0.84	0.08	0.28	0.03
RSES 181-2.10	3923	15.6	Holden *et al.*, 2009	2.36	0.11	0.37	0.04	0.16	0.02

RSES 56-3.17	3889	11	Bell and Harrison, 2013	2.48	0.28	0.51	0.05	0.21	0.03
Group II									
RSES 55-3.13	3862	5	Bell and Harrison, 2013	2.58	0.27	0.86	0.09	0.33	0.05
RSES 55-13.8	3885	7	Bell and Harrison, 2013	1.87	0.10	0.95	0.05	0.51	0.04
RSES 56-1.18	3843	4	Bell and Harrison, 2013	2.34	0.18	1.73	0.33	0.74	0.15
RSES 56-10.17	3870	5	Bell and Harrison, 2013	2.19	0.21	1.20	0.16	0.55	0.09
RSES 58-5.11	3871	4	Bell and Harrison, 2013	3.24	0.36	1.92	0.23	0.59	0.10
RSES 58-13.14	3892	7	Bell and Harrison, 2013	2.38	0.22	1.68	0.24	0.70	0.12
RSES 58-15.13	3893	4	Bell and Harrison, 2013	2.17	0.20	1.40	0.17	0.64	0.10
RSES 58-17.7	3910	6	Bell and Harrison, 2013	2.71	0.23	1.68	0.20	0.62	0.09
>3.9 Ga									
RSES 51-17.1	3950	6	Bell *et al.*, 2011	2.41	0.21	0.26	0.04	0.11	0.02
RSES 177-11.13	3977	6.1	Holden *et al.*, 2009	2.14	0.18	0.40	0.07	0.19	0.04
RSES 100-10.5	4078	8	Holden *et al.*, 2009	1.80	0.14	0.48	0.10	0.26	0.06
RSES 100-8.6	4054	7	Holden *et al.*, 2009	1.46	0.14	0.45	0.05	0.31	0.05
RSES 177-2.13	3994	6	Holden *et al.*, 2009	2.65	0.19	0.60	0.08	0.23	0.03
RSES 177-3.20	3982	13.2	Holden *et al.*, 2009	2.53	0.20	0.54	0.06	0.22	0.03
RSES 177-4.9	4021	5.6	Holden *et al.*, 2009	2.52	0.21	0.54	0.08	0.21	0.03
RSES 177-5.5	4047	7.2	Holden *et al.*, 2009	2.27	0.20	0.46	0.07	0.20	0.04
RSES 177-9.3	4094	11.5	Holden *et al.*, 2009	2.23	0.18	0.43	0.07	0.19	0.03
RSES 177-13.10	4026	8.4	Holden *et al.*, 2009	2.09	0.17	0.49	0.07	0.23	0.04
RSES 67-16.6	4038	12	Holden *et al.*, 2009	4.97	0.26	0.41	0.06	0.08	0.01
RSES 67-19.13	4041	14	Holden *et al.*, 2009	3.83	0.20	0.25	0.05	0.06	0.01
RSES 178-5.16	4059.7	3.3	Holden *et al.*, 2009	3.10	0.16	0.48	0.07	0.16	0.02
RSES 178-7.14	4012.3	18.0	Holden *et al.*, 2009	2.89	0.14	0.91	0.08	0.31	0.03
RSES 178-8.8	4073	5.5	Holden *et al.*, 2009	4.82	0.20	1.26	0.12	0.26	0.03
RSES 178-10.20	4037.1	15.3	Holden *et al.*, 2009	2.53	0.15	0.34	0.06	0.13	0.02
RSES 178-12.10	3990.5	7.3	Holden *et al.*, 2009	2.78	0.16	0.43	0.07	0.15	0.03
RSES 178-18.18	4109	12.5	Holden *et al.*, 2009	2.78	0.12	0.24	0.04	0.09	0.02
RSES 178-20.19	4009.3	4.0	Holden *et al.*, 2009	2.95	0.15	0.47	0.07	0.16	0.02
RSES 181-1.13	3966	7.9	Holden *et al.*, 2009	2.35	0.11	0.24	0.05	0.10	0.02
RSES 181-2.16	4064	6.8	Holden *et al.*, 2009	2.32	0.12	0.20	0.03	0.09	0.01
RSES 181-6.10	4150	4.1	Holden *et al.*, 2009	2.02	0.13	0.19	0.04	0.09	0.02
RSES 181-7.14	4159	6.1	Holden *et al.*, 2009	2.13	0.08	0.21	0.06	0.10	0.03
RSES 181-10.1	4026	11.1	Holden *et al.*, 2009	1.99	0.09	0.16	0.03	0.08	0.02
RSES 181-13.14	4139	13.9	Holden *et al.*, 2009	1.85	0.10	0.16	0.03	0.09	0.02
RSES 181-14.10	4133	7.1	Holden *et al.*, 2009	1.77	0.08	0.17	0.04	0.10	0.03
RSES 181-19.14	4021	11.4	Holden *et al.*, 2009	1.95	0.09	0.33	0.04	0.17	0.02

	F (μg/g)	2 s.e.	Cl (μg/g)	2 s.e.	Cl/F	2 s.e.
Average	2.28	0.19	0.54	0.11	0.24	0.04
Average in <3.8 Ga zircon	1.78	0.16	0.34	0.04	0.20	0.02
Average in 3.9–3.8 Ga zircon	**2.49**	**0.24**	**1.19**	**0.32**	**0.48**	**0.12**
Average in >3.9 Ga zircon	2.56	0.32	0.41	0.09	0.16	0.03
Average except Group II	2.25	0.21	0.39	0.06	0.18	0.02
Average of Group II	**2.44**	**0.28**	**1.43**	**0.33**	**0.59**	**0.12**
Granitic zircon	1.80	0.11	0.31	0.04	0.17	0.02

Table S-3 Crystallisation temperature, oxygen isotopic composition, and LREE classification in Jack Hills zircons.

Jack Hills Sample	$\delta^{18}O_{SMOW}$	2 s.e.	T(°C)	1 s.e.	FMQ	1 s.d.	Sm/La_N	1 s.d.	LREE-I	1 s.d.	LREE-I Classification	REE citation
<3.8 Ga												
RSES 51-4.2	5.32	0.34	692	19	-0.38	0.64	43.1	9.7	81.2	8.7	primary	Bell *et al.*, 2014
RSES 51-5.4	5.61	0.30	688	20	-3.65	0.70	11.7	3.5	133.8	21.9	primary	Bell *et al.*, 2014
RSES 51-5.7	5.90	0.31	694	15	2.71	0.57	76.0	14.9	89.6	8.4	primary	this study
RSES 51-6.2	5.52	0.32	684	15	2.19	0.59	89.0	21.3	126.6	9.5	primary	this study
RSES 51-6.9	5.55	0.29	693	15			193.6	60.1	110.6	20.6	primary	this study
RSES 51-10.10	5.89	0.31	656	15	1.72	0.58	147.4	34.1	85.3	8.2	primary	this study
RSES 51-10.11	5.39	0.32	684	15	-0.37	0.57	46.7	7.0	87.9	6.4	primary	this study
RSES 51-10.14			681	15	5.37	0.65	152.1	50.2	74.0	7.5	primary	this study
RSES 51-12.1			707	15	0.50	0.56	183.9	29.5	59.8	3.8	primary	this study
RSES 51-12.9	5.25	0.55	719	16	6.35	0.61	397.5	141.1	50.9	5.6	primary	this study
RSES 51-12.13	5.61	0.56	671	18	4.09	0.70	450.6	322.3	111.0	13.8	primary	this study
RSES 51-13.5			802	16			11.3	0.7	18.1	0.7	uncertain	this study
RSES 51-14.3			681	16	2.24	0.61	167.8	54.6	84.1	13.1	primary	this study
RSES 51-16.3	5.30	0.33	698	17	-2.85	0.59	108.2	33.5	34.1	4.5	primary	this study
RSES 51-4.7	5.16	0.31	676	19	5.13	0.64	19.5	4.8	85.8	14.0	primary	Bell *et al.*, 2014
RSES 51-11.1	6.06	0.56	709	19	7.79	0.64	280.7	71.3	44.8	3.5	primary	Bell *et al.*, 2014
RSES 51-16.1	5.50	0.29	704	19	6.06	0.65	33.9	8.4	52.8	6.2	primary	Bell *et al.*, 2014
RSES 51-4.1	5.95	0.30	648	38	4.99	0.85	71.2	75.4	68.6	24.9	primary	Bell *et al.*, 2014
RSES 195-1.15			695	39	3.21	0.74	83.8	16.8	55.2	3.6	primary	Bell *et al.*, 2014
RSES 181-5-2	5.24	0.17	652	16	-3.77	0.58	17.8	3.6	67.9	8.7	primary	Bell *et al.*, 2014
3.9–3.8 Ga												
Group I												
RSES 178-20.20	6.48	0.24	766	17	-4.52	0.59	17.0	5.0	60.6	15.1	primary	this study
RSES 181-2.10	6.18	0.20	701	16	-0.60	0.62	18.5	4.0	46.2	8.7	primary	this study
RSES 56-3.17			623	20	-2.35	0.66	71.7	18.0	59.0	4.9	primary	Bell and Harrison, 2013
Group II												
RSES 55-3.13			589	29	2.68	0.65	253.6	137.1	174.8	54.5	primary	Bell and Harrison, 2013
RSES 55-13.8	4.77	0.33	538	33	-5.90	1.44	24.2	20.4	414.8	347.9	primary	Bell and Harrison, 2013
RSES 56-1.18	6.47	0.64	577	27	-6.67	0.91	28.5	13.1	126.1	27.4	primary	Bell and Harrison, 2013
RSES 56-10.17	6.31	1.17	592	23	-5.58	0.75	40.6	10.6	249.6	62.8	primary	Bell and Harrison, 2013
RSES 58-5.11	4.57	0.33	580	21	-4.61	0.80	27.0	7.7	191.8	46.3	primary	Bell and Harrison, 2013
RSES 58-13.14	6.35	0.22	610	20	-4.30	0.76	69.1	19.2	184.7	75.3	primary	Bell and Harrison, 2013
RSES 58-15.13	6.16	0.09	610	20	-4.37	0.74	63.6	17.6	135.1	19.9	primary	Bell and Harrison, 2013
RSES 58-17.7	5.89	0.19	573	22	-5.04	0.82	48.9	16.1	553.0	283.9	primary	Bell and Harrison, 2013
>3.9 Ga												
RSES 51-17.1	5.85	0.30	686	19	-0.86	0.69	350.8	106.7	49.8	4.1	primary	Bell *et al.*, 2014
RSES 177-11.13	6.04	0.24	652	17	-3.08	0.62	13.6	3.1	134.8	98.2	primary	this study
RSES 100-10.5	5.94	0.26	676	30	-5.11	0.76	142.0	52.0	30.5	2.5	primary	Bell and Harrison, 2013
RSES 100-8.6			670	37	0.28	1.14	64.3	61.3	59.6	20.9	primary	Bell and Harrison, 2013
RSES 177-2.13	5.90	0.18	716	16	0.86	0.58	24.8	4.3	84.2	10.7	primary	this study
RSES 177-3.20	6.00	0.16	711	16	-4.45	0.59	18.0	4.5	57.9	7.8	primary	this study
RSES 177-4.9	5.65	0.20	720	25	-4.47	0.63	41.3	13.2	55.8	11.1	primary	this study
RSES 177-5.5	5.96	0.14	674	16	0.55	0.59	32.0	9.1	165.1	48.5	primary	this study
RSES 177-9.3	6.69	0.13	701	16	0.20	0.59	48.4	9.3	116.5	18.2	primary	this study

RSES 177-13.10	6.03	0.17	687	16	-4.72	0.59	23.5	5.9	164.3	68.0	primary	this study
RSES 67-16.6	7.26	0.69										
RSES 67-19.13	6.62	0.69	652	28	1.04	0.93	227.1	141.6	70.4	16.8	primary	Bell and Harrison, 2013
RSES 178-5.16	5.72	0.23	655	20	-4.06	0.61	33.6	7.1	133.0	31.8	primary	this study
RSES 178-7.14	6.78	0.21	747	17	1.54	0.60	36.7	8.6	51.1	8.9	primary	this study
RSES 178-10.20	6.00	0.20	682	17	-0.50	0.60	42.0	8.3	46.8	4.1	primary	this study
RSES 178-12.10	7.16	0.23	706	14	-2.34	0.56	57.6	6.4	73.6	4.8	primary	this study
RSES 178-18.18	5.85	0.19	726	35	-1.01	0.80	13.2	6.1	63.3	7.6	primary	this study
RSES 178-20.19	6.35	0.22	688	16	1.64	0.63	39.0	6.6	133.6	40.6	primary	this study
RSES 181-1.13	4.66	0.18	703	17	-5.48	0.60	26.9	5.3	100.4	16.9	primary	this study
RSES 181-2.16	6.31	0.27	669	16	-1.03	0.59	39.2	7.4	114.7	18.3	primary	this study
RSES 181-6.10	5.16	0.19	683	16	0.44	0.61	37.9	7.8	100.9	13.5	primary	this study
RSES 181-7.14	5.02	0.22	752	16	2.50	0.56	12.3	0.9	42.3	3.3	primary	this study
RSES 181-10.1	6.86	0.24	714	16	-3.81	0.58	41.5	9.8	47.3	5.6	primary	this study
RSES 181-13.14	6.33	0.25	683	14	-1.97	0.56	104.1	12.9	52.8	2.8	primary	this study
RSES 181-14.10	5.06	0.19	725	16	-0.16	0.58	45.2	9.0	67.5	10.8	primary	this study
RSES 181-19.14	6.19	0.22	698	14	-4.32	0.56	43.20	7.24	74.58	6.39	primary	this study

Table S-4 REE in Jack Hills zircons, the references of REE data are shown in Table S-3.

Jack Hills							REE normalised to CI							
Sample	**La**	**Ce**	**Pr**	**Nd**	**Sm**	**Eu**	**Gd**	**Tb**	**Dy**	**Ho**	**Er**	**Tm**	**Yb**	**Lu (N)**
<3.8 Ga														
RSES 51-4.2	0.40	23.40	1.19	2.81	17.41	6.85	80.64	165.56	282.65	507.79	820.71	1152.13	1511.91	2193.36
RSES 51-5.4	0.73	12.59	1.03	1.45	8.54	1.13	50.79	124.69	236.82	499.05	779.89	1112.72	1552.39	2174.73
RSES 51-5.7	0.19	23.68	0.53	1.80	14.07	5.88	57.90	124.63	214.38	401.99	631.41	869.38	1188.59	1758.42
RSES 51-6.2	0.24	23.62	0.45	2.64	21.65	2.95	106.51	247.81	451.47	847.57	1257.35	1732.41	2312.70	3409.43
RSES 51-6.9	0.14	32.57	0.16	1.10	27.39	3.25	45.48	110.49	200.38	388.44	605.65	911.00	1240.80	1936.51
RSES 51-10.10	0.23	33.29	0.79	2.56	33.34	3.96	82.29	193.67	328.16	610.24	949.63	1305.94	1675.32	2496.97
RSES 51-10.11	0.42	24.34	1.08	3.16	19.68	6.11	82.78	192.22	344.79	663.09	1035.79	1461.42	1959.71	3007.40
RSES 51-10.14	0.23	30.89	0.14	2.39	35.44	5.03	69.55	158.41	271.37	493.45	762.25	1065.23	1447.15	2134.45
RSES 51-12.1	0.38	32.55	1.95	8.26	69.24	11.03	195.54	413.59	670.71	1162.91	1667.89	2176.96	2773.43	3919.51
RSES 51-12.9	0.10	44.69	0.74	5.27	39.44	6.43	100.76	201.77	352.70	628.91	908.60	1185.93	1568.27	2280.76
RSES 51-12.13	0.04	21.25	0.63	2.88	18.79	7.09	86.78	229.49	403.40	754.04	1171.42	1778.37	2284.05	3824.00
RSES 51-13.5	4.49	57.56	18.2	22.77	50.68	23.49	101.25	218.64	321.06	546.69	793.25	1078.75	1493.23	2154.00
RSES 51-14.3	0.14	13.61	0.24	1.33	23.43	3.99	39.40	97.50	176.77	332.13	505.59	787.28	1060.28	1640.41
RSES 51-16.3	0.18	7.38	1.11	2.94	19.00	11.83	38.88	71.22	126.13	223.07	347.62	534.13	739.57	1371.03
RSES 51-4.7	0.49	18.62	0.67	1.77	9.62	7.16	52.44	107.22	179.91	340.93	513.48	724.44	966.29	1457.58
RSES 51-11.1	0.30	54.99	3.65	16.29	84.12	14.95	297.34	552.30	848.61	1389.78	1932.88	2463.42	3045.26	4349.83
RSES 51-16.1	0.41	30.16	2.29	2.78	13.88	5.40	44.52	90.73	168.61	310.53	503.81	687.23	921.45	1485.23
RSES 51-4.1	0.19	23.36	0.40	2.51	13.66	0.00	57.09	120.84	203.85	455.02	705.20	794.55	1112.79	1702.93
RSES 195-1.15	0.27	42.87	1.55	4.80	22.84	9.59	105.42	174.89	298.71	530.46	768.46	1065.51	1451.94	2101.92
RSES 181-5-2	0.44	12.59	1.01	2.24	7.86	2.16	29.24	73.93	150.38	286.68	453.26	733.62	998.62	1514.93
3.9–3.8 Ga														
Group I														
RSES 178-20.20	0.32	3.25	0.76	0.85	5.48	2.67	15.43	39.41	64.73	121.18	199.37	291.34	401.76	581.71
RSES 181-2.10	0.39	14.64	0.63	1.93	7.19	3.49	25.77	53.85	90.63	166.93	261.81	371.13	524.58	789.07
RSES 56-3.17	0.25	20.50	1.33	3.73	17.99	4.47	63.57	140.77	249.32	466.20	685.96	945.09	1322.51	1912.40

Group II														
RSES 55-3.13	0.08	8.36	0.48	2.02	21.40	7.33	125.67	296.37	506.98	884.84	1252.41	1677.65	2007.29	2836.05
RSES 55-13.8	0.08	2.35	0.07	0.12	1.88	1.23	13.61	38.34	78.54	167.16	278.60	471.60	717.23	1143.57
RSES 56-1.18	0.18	3.98	0.29	1.05	5.17	1.54	29.25	76.54	151.18	307.71	464.78	704.40	1010.76	1504.00
RSES 56-10.17	0.26	5.56	0.30	0.61	10.58	3.89	57.51	130.85	238.62	430.41	671.60	951.72	1281.17	1786.89
RSES 58-5.11	0.23	5.54	0.16	0.54	6.11	1.97	31.61	80.22	150.37	261.76	405.83	600.04	813.37	1214.84
RSES 58-13.14	0.19	5.28	0.26	0.93	13.36	4.72	71.25	159.88	263.59	424.51	612.66	779.36	1024.44	1405.82
RSES 58-15.13	0.20	5.43	0.26	1.40	13.00	5.15	68.06	162.58	263.15	471.09	655.73	874.72	1132.20	1603.96
RSES 58-17.7	0.19	4.57	0.14	0.28	9.31	1.31	53.76	130.63	259.55	515.44	847.00	1289.35	1880.89	2948.49
>3.9 Ga														
RSES 51-17.1	0.17	20.36	2.57	10.65	58.41	8.23	199.70	397.04	630.22	1102.72	1573.11	2054.81	2608.60	3628.54
RSES 177-11.13	0.36	5.83	0.18	0.36	4.93	2.36	17.69	40.56	72.88	144.36	217.65	354.81	490.82	827.84
RSES 100-10.5	0.67	28.37	10.2	28.46	95.40	10.01	232.73	495.62	839.34	1375.20	1750.35	2204.55	2555.84	3305.01
RSES 100-8.6	0.18	16.51	0.65	2.46	11.69	4.75	49.74	92.73	165.10	281.17	411.57	578.49	727.42	1235.45
RSES 177-2.13	0.61	30.54	1.01	3.03	15.07	3.47	64.46	156.28	292.05	570.00	904.33	1204.07	1725.49	2508.14
RSES 177-3.20	0.76	9.52	1.23	2.80	13.71	6.74	52.02	115.55	184.88	346.50	519.91	800.49	1113.70	1564.17
RSES 177-4.9	0.47	6.32	1.00	2.48	19.46	23.19	72.78	130.83	184.17	245.21	255.47	278.83	297.86	383.02
RSES 177-5.5	0.31	20.45	0.55	1.16	9.95	6.23	59.65	145.65	261.69	492.37	775.65	1126.72	1558.71	2327.34
RSES 177-9.3	0.39	19.69	0.73	3.05	19.11	6.73	104.57	253.39	442.36	797.95	1155.72	1511.84	1978.71	2690.45
RSES 177-13.10	0.32	4.29	0.47	0.73	7.44	3.03	38.22	97.96	170.53	318.24	487.26	693.95	926.46	1465.10
RSES 67-19.13	0.08	17.78	0.81	2.67	19.17	11.30	59.31	119.53	244.42	376.80	586.71	815.47	977.18	1616.23
RSES 178-5.16	0.46	9.84	0.72	1.73	15.60	4.80	73.97	177.30	318.98	610.78	988.94	1364.57	1944.67	2985.27
RSES 178-7.14	0.48	20.55	0.63	2.76	17.65	3.85	53.45	111.88	176.94	314.20	482.91	658.34	935.26	1392.33
RSES 178-10.20	0.38	23.61	1.19	4.04	15.77	7.57	61.31	119.77	195.87	354.34	521.81	742.53	948.89	1476.88
RSES 178-12.10	0.34	10.05	0.92	3.21	19.37	6.74	79.69	174.23	290.64	528.12	755.19	1024.91	1370.32	2006.75
RSES 178-18.18	0.61	17.50	1.02	2.33	8.11	3.45	38.63	84.90	145.29	291.19	485.09	724.92	1073.75	1693.08
RSES 178-20.19	0.40	21.92	0.34	2.15	15.63	2.51	77.70	193.01	374.55	712.62	1114.64	1620.76	2210.40	3236.59
RSES 181-1.13	0.43	4.07	0.61	1.83	11.43	5.25	54.78	118.76	228.11	427.22	663.29	945.36	1325.25	2044.71
RSES 181-2.16	0.36	16.30	0.63	2.34	14.24	8.00	69.24	167.06	330.48	584.89	921.20	1345.64	1833.43	2784.19
RSES 181-6.10	0.33	17.23	0.45	2.54	12.35	4.34	71.31	159.86	291.07	558.57	854.55	1248.24	1718.69	2510.33
RSES 181-7.14	2.82	35.69	7.02	9.46	34.71	12.42	112.44	231.92	403.93	720.11	1118.99	1683.34	2313.79	3416.66
RSES 181-10.1	0.36	6.38	0.88	3.64	14.75	10.57	60.73	112.09	181.52	319.66	476.65	691.09	956.38	1543.69
RSES 181-13.14	0.26	12.68	1.10	5.09	27.14	16.84	98.31	204.45	316.60	558.34	814.00	1102.07	1486.85	2280.96
RSES 181-14.10	0.34	15.46	0.90	2.29	15.46	5.81	50.13	114.66	197.07	361.11	569.15	826.44	1116.45	1668.03
RSES 181-19.14	0.14	4.68	0.31	1.04	6.19	2.80	25.23	58.03	94.96	191.61	294.96	446.86	658.78	1157.52

Supplementary Information References

Amelin, Y. (1998) Geochronology of the Jack Hills detrital zircons by precise U–Pb isotope dilution analysis of crystal fragments. *Chemical Geology* 146, 25-38.

Amelin, Y., Der-Chuen, L., Halliday, A.N., Pidgeon, R.T. (1999) Nature of the Earth's earliest crust from hafnium isotopes in single detrital zircons. *Nature* 399, 252-255.

Barth, A.P., Wooden, J.L., Mueller, P.A., Economos, R.C. (2016) Granite provenance and intrusion in arcs: Evidence from diverse zircon types in Big Bear Lake Intrusive Suite, USA. *Lithos* 246, 261-278.

Bell, E.A., Harrison, T.M. (2013) Post-Hadean transitions in Jack Hills zircon provenance: A signal of the Late Heavy Bombardment? *Earth and Planetary Science Letters* 364, 1-11.

Bell, E.A., Boehnke, P., Harrison, T.M. (2016) Recovering the primary geochemistry of Jack Hills zircons through quantitative estimates of chemical alteration. *Geochimica et Cosmochimica Acta* 191, 187-202.

Bell, E.A., Harrison, T.M., Kohl, I.E., Young, E.D. (2014) Eoarchean crustal evolution of the Jack Hills zircon source and loss of Hadean crust. *Geochimica et Cosmochimica Acta* 146, 27-42.

Bell, E.A., Harrison, T.M., McCulloch, M.T., Young, E.D. (2011) Early Archean crustal evolution of the Jack Hills Zircon source terrane inferred from Lu–Hf, $^{207}Pb/^{206}Pb$, and $\delta^{18}O$ systematics of Jack Hills zircons. *Geochimica et Cosmochimica Acta* 75, 4816-4829.

Bell, E.A., Boehnke, P., Harrison, T.M. (2017) Applications of biotite inclusion composition to zircon provenance determination. *Earth and Planetary Science Letters* 473, 237-246.

Burnett, D.S., Jurewicz, A.J., Woolum, D.S., Wang, J., Paque, J.M., Nittler, L.R., McKeegan, K.D., Humayun, M., Hervig, R., Heber, V.S., Guan, Y. (2015) Ion Implants as Matrix-Appropriate Calibrators for Geochemical Ion Probe Analyses. *Geostandards and Geoanalytical Research*, 39, 265-276.

Cavosie, A.J., Wilde, S.A., Liu, D., Weiblen, P.W., Valley, J.W. (2004) Internal zoning and U–Th–Pb chemistry of Jack Hills detrital zircons: a mineral record of early Archean to Mesoproterozoic (4348–1576 Ma) magmatism. *Precambrian Research* 135, 251-279.

Cavosie, A.J., Valley, J.W., Wilde, S.A. (2005) Magmatic $\delta^{18}O$ in 4400–3900 Ma detrital zircons: A record of the alteration and recycling of crust in the Early Archean. *Earth and Planetary Science Letters* 235, 663-681.

Chappell, B.W. (1974) Two contrasting granite types. *Pacific Geology* 8, 173-174.

Chappell, B.W., Simpson, P.R. (1984) Source rocks of I-and S-type granites in the Lachlan Fold Belt, southeastern Australia. *Philosophical Transactions of the Royal Society London A* 310, 693-707.

Chappell, B.W., White, A.J.R., Wyborn, D., (1987) The importance of residual source material (restite) in granite petrogenesis. *Journal of Petrology* 28, 1111-1138.

Chappell, B.W., White, A.J.R.., Williams, I.S. (1990) Excursion Guide B-1, Cooma Granidiorite and Berridale Batholith. In *Seventh International Conference on Geochronology, Cosmochronology, and Isotope Geology*, 1–53, Bureau of Mineral Resources, Record 1990/50, Geology and Geophysics, Australia.

Chappell, B.W., White, A.J.R., Wyborn, D. (1993) The Cowra Granodiorite and its enclaves. Excursion guide, *Australian Geological Survey Org. Rec.* 67, IAVCEI Canberra, Canberra.

Chase, A.B., Osmer, J.A. (1966) Growth and preferential doping of zircon and thorite. *Journal of the Electrochemical Society* 113, 198-199.

Compston, W., Pidgeon, R. T. (1986) Jack Hills, evidence of more very old detrital zircons in Western Australia. *Nature* 321, 766–769.

Griffin, T. J., White, A. R., Chappell, B. W. (1978) The Moruya batholith and geochemical contrasts between the Moruya and Jindabyne suites. *Journal of Geological Society of Australian* 25, 235–247.

Hanchar, J.M., Finch, R.J., Hoskin, P.W., Watson, E.B., Cherniak, D.J., Mariano, A.N. (2001) Rare earth elements in synthetic zircon: Part 1. Synthesis, and rare earth element and phosphorus doping. *American Mineralogist* 86, 667-680.

Hine, R., Williams, I. S., Chappell, B. W., White, A. J. R. (1978) Contrasts between I- and S-type granitoids of the Kosciusko Batholith, *Journal of Geological Society of Australian* 25, 219–234.

Holden, P., Lanc, P., Ireland, T.R., Harrison, T.M., Foster, J.J., Bruce, Z. (2009) Mass-spectrometric mining of Hadean zircons by automated SHRIMP multi-collector and single-collector U/Pb zircon age dating: The first 100,000 grains. *International Journal of Mass Spectrometry* 286, 53-63.

Joyce, A. S. (1973) Application of cluster analysis to detection of subtle variation in a granitic intrusion. *Chemical Geology* 11, 297–306.

Leta, D.P., Morrison, G.H. (1980) Ion implantation for in-situ quantitative ion microprobe analysis. *Analytical Chemistry* 52, 277-280.

Maas, R., Kinny, P.D., Williams, I.S., Froude, D.O., Compston, W. (1992) The Earth's oldest known crust: a geochronological and geochemical study of 3900–4200 Ma old detrital zircons from Mt. Narryer and Jack Hills, Western Australia. *Geochimica et Cosmochimica Acta 56*, 1281-1300.

Mojzsis, S.J., Harrison, T.M., Pidgeon, R.T. (2001) Oxygen-isotope evidence from ancient zircons for liquid water at the Earth's surface 4,300 Myr ago. *Nature,* 409, 178.

Phillips, G. N., Wall, V. J., Clemens, J. D. (1981) Petrology of the Strathbogie Batholigh: A Cordierite-bearing granite. *The Canadian. Mineralogist* 19, 47–63.

Silver, L.T., Chappell, B.W. (1988) The Peninsular Ranges Batholith: an insight into the evolution of the Cordilleran batholiths of southwestern North America. *Earth and Environmental Science Transactions of The Royal Society of Edinburgh* 79, 105-121.

Spaggiari, C.V., Pidgeon, R.T., Wilde, S.A. (2007) The Jack Hills greenstone belt, Western Australia: part 2: lithological relationships and implications for the deposition of≥ 4.0 Ga detrital zircons. *Precambrian Research* 155, 261-286.

Steele, R.C., Heber, V.S., McKeegan, K.D. (2017) Matrix effects on the relative sensitivity factors for manganese and chromium during ion microprobe analysis of carbonate: Implications for early Solar System chronology. *Geochimica et Cosmochimica Acta* 201, 245-259.

Suzuki, K., Kouta, H., Nagasawa, H. (1992) Hf-Zr interdiffusion in single crystal zircon. *Geochemical Journal* 26, 99-104.

Todd, V.R., Shaw, S.E., Hammarstrom, J.M., Johnson, S.E. (2003) Cretaceous plutons of the Peninsular Ranges batholith, San Diego and westernmost Imperial counties, California: Intrusion across a Late Jurassic continental margin. *Special Papers-Geological Society of America,* 185-236.

Trail, D., Mojzsis, S. J., Harrison, T. M. (2007) Thermal events documented in Hadean zircons by ion microprobe depth profiles, *Geochimica et Cosmochimica Acta* 71, 4044–4065.

Trail. D., Cherniak, D.J., Watson, E.B., Harrison, T.M., Weiss, B.P., Szumila. I. (2016) Li zoning in zircon as a potential geospeedometer and peak temperature indicator. *Contributions to Mineralogy and Petrology* 171, 25-40.

Trail, D., Tailby, N., Wang, Y., Harrison, T.M., Boehnke, P. (2017) Aluminum in zircon as evidence for peraluminous and metaluminous melts from the Hadean to present. *Geochemistry, Geophysics, Geosystems* 18, 1580-1593.

White, A.J.R., Chappell, B.W. (1983) Granitoid types and their distribution in the Lachlan Fold Belt, southeastern Australia. *Geological Society of America Memoir* 159, 21-34.

Ziegler, J.F. (2004) SRIM-2003. *Nuclear instruments and methods in physics research section B: Beam interactions with materials and atoms* 219, 1027-1036.

Zinner, E., Walker, R.M. (1975) Ion-probe studies of artificially implanted ions in lunar samples. *Lunar and Planetary Science Conference Proceedings* 6, 3601-3617.